Article

Molecular Cell

Cross-Regulation between TDP-43 and Paraspeckles Promotes Pluripotency-Differentiation Transition

Graphical Abstract

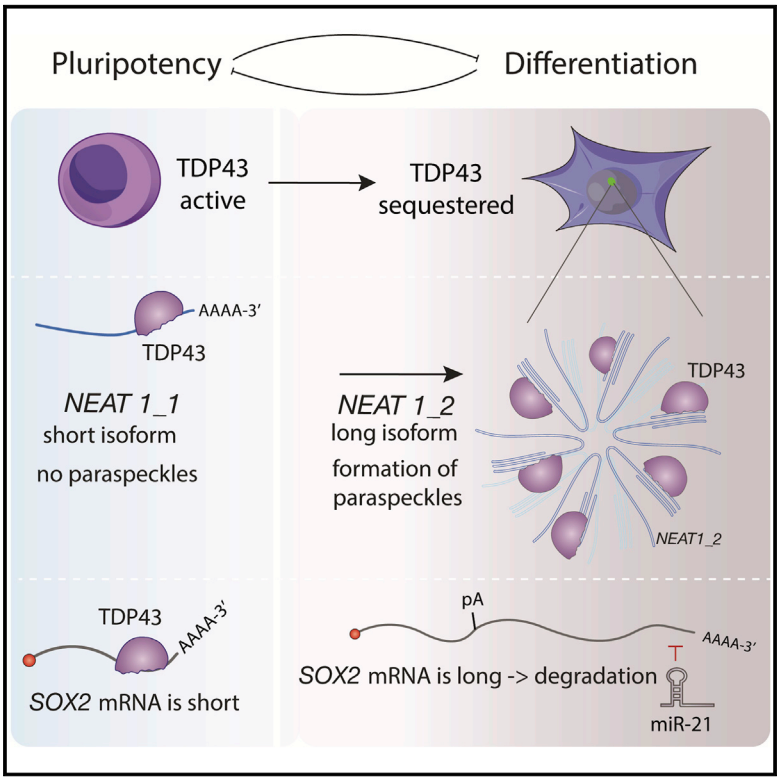

Highlights

- TDP-43 maintains pluripotency by regulating expression of pluripotency factors
- TDP-43 represses formation of paraspeckles in ESCs by regulating *Neat1*
- The paraspeckle-inducing isoform of *Neat1* promotes differentiation of ESCs and embryos
- Cross-regulation between TDP-43 and *Neat1* enhances pluripotency-differentiation axis

Authors

Miha Modic, Markus Grosch, Gregor Rot, ..., Tetsuro Hirose, Jernej Ule, Micha Drukker

Correspondence

jernej.ule@crick.ac.uk (J.U.), micha.drukker@helmholtz-muenchen.de (M.D.)

In Brief

Modic et al. uncover opposing roles of TDP-43 and paraspeckles in pluripotency and differentiation that are further enhanced by their cross-regulation. TDP-43 represses paraspeckles through processing of the scaffolding lncRNA *Neat1*, whereas paraspeckles partially sequester TDP-43. This reciprocal relationship promotes coordinated changes in alternative polyadenylation essential for efficient exit from pluripotency.

Modic et al., 2019, Molecular Cell *74*, 951–965
June 6, 2019 © 2019 The Authors. Published by Elsevier Inc.
https://doi.org/10.1016/j.molcel.2019.03.041

CellPress

Molecular Cell
Article

Cross-Regulation between TDP-43 and Paraspeckles Promotes Pluripotency-Differentiation Transition

Miha Modic,[1,3,4] Markus Grosch,[1] Gregor Rot,[5] Silvia Schirge,[1,6] Tjasa Lepko,[1] Tomohiro Yamazaki,[7] Flora C.Y. Lee,[3,4] Ejona Rusha,[1] Dmitry Shaposhnikov,[1] Michael Palo,[3,4] Juliane Merl-Pham,[8] Davide Cacchiarelli,[9,10,11] Boris Rogelj,[12,13,14] Stefanie M. Hauck,[8] Christian von Mering,[5] Alexander Meissner,[9,10,15] Heiko Lickert,[1,6] Tetsuro Hirose,[7] Jernej Ule,[3,4,*] and Micha Drukker[1,2,16,*]
[1]Institute of Stem Cell Research, Helmholtz Zentrum München, 85764 Neuherberg, Germany
[2]Comprehensive Pneumology Center (CPC-M), Ludwig-Maximilians-Universität München, Asklepios Fachkliniken München-Gauting und Helmholtz Zentrum München, Max-Lebsche-Platz 31, 81377 Munich, Germany
[3]The Francis Crick Institute, London NW1 1AT, UK
[4]Department for Neuromuscular Diseases, UCL Queen Square Institute of Neurology, London WC1N 3BG, UK
[5]Institute of Molecular Life Sciences of the University of Zurich and Swiss Institute of Bioinformatics, 8057 Zurich, Switzerland
[6]Institute of Diabetes and Regeneration Research, Helmholtz Zentrum München, 85764 Neuherberg, Germany
[7]Institute for Genetic Medicine, Hokkaido University, Sapporo 060-0815, Japan
[8]Research Unit Protein Science, Helmholtz Zentrum München, German Research Center for Environmental Health GmbH, 80939 Munich, Germany
[9]Broad Institute of Harvard University/MIT, Cambridge, MA 02142, USA
[10]Department of Stem Cell and Regenerative Biology, Harvard University, Cambridge, MA 02138, USA
[11]Telethon Institute of Genetics and Medicine (TIGEM), NA 80078 Pozzuoli, Italy
[12]Department of Biotechnology, Jožef Stefan Institute, 1000 Ljubljana, Slovenia
[13]Faculty of Chemistry and Chemical Technology, University of Ljubljana, 1000 Ljubljana, Slovenia
[14]Biomedical Research Institute BRIS, 1000 Ljubljana, Slovenia
[15]Department of Genome Regulation, Max Planck Institute for Molecular Genetics, 14195 Berlin, Germany
[16]Lead Contact
*Correspondence: jernej.ule@crick.ac.uk (J.U.), micha.drukker@helmholtz-muenchen.de (M.D.)
https://doi.org/10.1016/j.molcel.2019.03.041

SUMMARY

RNA-binding proteins (RBPs) and long non-coding RNAs (lncRNAs) are key regulators of gene expression, but their joint functions in coordinating cell fate decisions are poorly understood. Here we show that the expression and activity of the RBP TDP-43 and the long isoform of the lncRNA *Neat1*, the scaffold of the nuclear compartment "paraspeckles," are reciprocal in pluripotent and differentiated cells because of their cross-regulation. In pluripotent cells, TDP-43 represses the formation of paraspeckles by enhancing the polyadenylated short isoform of *Neat1*. TDP-43 also promotes pluripotency by regulating alternative polyadenylation of transcripts encoding pluripotency factors, including *Sox2*, which partially protects its 3′ UTR from *miR-21*-mediated degradation. Conversely, paraspeckles sequester TDP-43 and other RBPs from mRNAs and promote exit from pluripotency and embryonic patterning in the mouse. We demonstrate that cross-regulation between TDP-43 and *Neat1* is essential for their efficient regulation of a broad network of genes and, therefore, of pluripotency and differentiation.

INTRODUCTION

A long noncoding RNA (lncRNA) called *NEAT1* acts as a scaffold for paraspeckles by recruiting many RNA-binding proteins (RBPs) that have been implicated in development, cancer, and neurodegeneration, including TDP-43 and FUS (West et al., 2016). Paraspeckles have been implicated in post-transcriptional regulation by association with specific mRNAs and RBPs (Chen and Carmichael, 2009; Hennig et al., 2015; Jiang et al., 2017; Naganuma et al., 2012; Prasanth et al., 2005). Remarkably, paraspeckles have been identified in many types of somatic cells but not in embryonic stem cells (ESCs) (Chen and Carmichael, 2009). Several lncRNAs and RBPs can affect differentiation of ESCs by regulating gene expression (Flynn and Chang, 2014), but the role of their cross-regulation in promoting efficient transitions during differentiation is unknown. Thus, investigating the recruitment of specific RBPs by *NEAT1* into paraspeckles in the context of ESC differentiation can answer the larger question of how the scaffolding of RBPs by lncRNAs is coupled to cell fate transitions and how this might coordinate the broader gene regulatory networks that establish distinct cell identities.

Here we reveal the importance of cross-regulation between *NEAT1* and TDP-43 in the context of cellular differentiation. We find that an evolutionarily conserved switch in alternative polyadenylation (APA) of *NEAT1* is regulated by TDP-43 and leads to induction of the long isoform (*NEAT1_2*), which scaffolds

This is an open access article under the CC BY-NC-ND license (http://creativecommons.org/licenses/by-nc-nd/4.0/).

paraspeckles upon exit from pluripotency. We also show that TDP-43 and *NEAT1_2* have opposing functions during differentiation because of their cross-regulation: TDP-43 represses the formation of paraspeckles in pluripotent cells, whereas *NEAT1* partly sequesters TDP-43 away from mRNAs in differentiated cells. TDP-43 also globally regulates the APA of many mRNAs encoding pluripotency regulators, including the core pluripotency and reprogramming factor *Sox2*. We demonstrate that their cross-regulation is essential for the efficient functions of TDP-43 and *Neat1* in promoting states of pluripotency and differentiation, respectively. This shows how a lncRNA can act together with cross-regulated RBPs to increase the efficiency of cell fate transitions.

RESULTS

APA Induces Formation of Paraspeckles upon Exit from Pluripotency

The *NEAT1* gene produces two transcripts, a short isoform that is polyadenylated and does not form paraspeckles (*NEAT1_1*) and a full-length isoform that ends with a triple helix and forms paraspeckles that scaffold various RBPs (*NEAT1_2*) (Li et al., 2017; Naganuma et al., 2012). We quantified *NEAT1* foci in human ESCs (hESCs) that were prompted to differentiate to diverse fates using single-molecule fluorescence *in situ* hybridization (FISH) probes that recognized either the region common to both isoforms or the region specific to *NEAT1_2* (Figure S1A). We observed a dramatic lineage-independent increase in the number of *NEAT1_2* foci in the early trophoblast-, mesoderm, mesendoderm-, and neuroectoderm-differentiated progeny of hESCs (Figure 1A; Figure S1B) and determined that removal of pluripotency medium (spontaneous differentiation) is sufficient to trigger paraspeckle formation (Figure 1A). As evidence of a conserved mechanism, removal of pluripotency maintenance factors (2iLIF) from the medium was also sufficient to trigger paraspeckle formation in mouse ESCs (mESCs) (Figure 1B; Figure S1C).

To gain insights into the mechanism that contributes to *NEAT1* dynamics, we sequenced RNAs from undifferentiated hESCs and their progeny. Sequencing of nascent RNA (nascent RNA-seq) by selecting for transcripts pulse-labeled with ethynyl uridine revealed that *NEAT1_1* is expressed in undifferentiated hESCs, and *NEAT1_2* was found among the 18 transcripts that were commonly upregulated within 24 h differentiation treatment by WNT3A, a small-molecule inhibitor of GSK3 (CHIR99021), and BMP4 (Figure 1C; Figure S1D; Table S1). As reported for somatic cells (Mao et al., 2011; Shevtsov and Dundr, 2011), we found that *NEAT1_2* is localized to the chromatin, whereas *NEAT1_1* is localized to the nucleoplasm (Figures S1E–S1J). To determine whether the expression of *NEAT1* is post-transcriptionally regulated, we used CRISPR/Cas9-mediated editing to delete the internal polyadenylation (*ΔpA*) site of *NEAT1* in hESCs and of *Neat1* in mESCs. We found that this induced the production of *NEAT1_2* in undifferentiated hESCs or mESCs (Figures 1D, 1E, S2A, and S2B).

We found previously that *NEAT1* is strongly bound by TDP-43 in somatic cells (Tollervey et al., 2011), which led us to inquire whether this RBP regulates *NEAT1*. Indeed, we found that overexpression of TDP-43 repressed paraspeckle formation upon spontaneous differentiation of mESCs (Figure 1B; Figure S1C). Conversely, depletion of *TDP-43* induced the production *NEAT1_2* and paraspeckle formation in hESCs or mESCs to a similar extent as deletion of the pA site, as detected by single-molecule imaging and RNA-seq (Figures 1D–1F; Figure S2C). We conclude that the isoform switch of *NEAT1* is regulated by TDP-43 to coincide with the exit from pluripotency, ensuring that *NEAT1_2* scaffolds paraspeckles upon differentiation irrespective of the embryonic lineage.

NEAT1_2 Recruits TDP-43 into Paraspeckles and Away From mRNAs

Because TDP-43 is a known paraspeckle RBP (West et al., 2016), we next asked whether reciprocal regulation by *NEAT1_2* on TDP-43 takes place upon early differentiation. We used a global mRNA-RBP occupancy analysis (Baltz et al., 2012; Castello et al., 2012) to examine how induction of *NEAT1_2* in the undifferentiated state of *NEAT1ΔpA* hESCs affects the binding of RBPs to polyadenylated mRNAs (Figure 1D; Figures S2D and S2E). Because *NEAT1_2* is not polyadenylated, it remains present in the supernatant after the removal of polyadenylated mRNAs (Figure S2F). Thus, the RBPs that are recruited to paraspeckles and crosslinked to *NEAT1_2* in *NEAT1ΔpA* hESCs are not expected to co-purify with polyadenylated mRNAs, and, as a result, their mRNA occupancy is expected to decrease (Figure 2A). Indeed, the mRNA occupancy of known paraspeckle proteins, including TDP-43, NONO, SFPQ, RBM14, HNRNPH3, HNRNPK, FUS, and DAZAP1 (Fox et al., 2018), was decreased in *NEAT1ΔpA* hESCs (Figure 2B; Figure S2G; Table S2), demonstrating that induction of *NEAT1_2* indeed leads to partial recruitment of a cohort of RBPs into paraspeckles and away from mRNAs. In addition, we found that TDP-43, but not control RBPs, was increasingly retained in the supernatant after depletion of polyadenylated mRNAs in *NEAT1ΔpA* hESCs (Figure 2C), confirming a role of *NEAT1_2* in sequestering TDP-43 into paraspeckles.

TDP-43 is known to be localized to the outer shell of paraspeckles (Naganuma et al., 2012; West et al., 2016), but it has been unclear whether TDP-43 needs to bind to *NEAT1_2* to localize to paraspeckles. The *NEAT1_2* isoform contains three regions rich in UGUG repeats that overlap with the main peaks of TDP-43 binding (Tollervey et al., 2011). We used CRISPR-Cas9 editing in the HAP1 cell line, which forms paraspeckles in the steady state, to delete these three regions from the endogenous *NEAT1* gene (Figure 2D; *NEAT1ΔUG*) that are not essential for paraspeckle assembly (Yamazaki et al., 2018). We confirmed that *NEAT1* foci formation and assembly of PSPC1 in paraspeckles remained intact in *NEAT1ΔUG* cells (Figure 2E). In contrast, localization of TDP-43 into paraspeckles dramatically decreased in *NEAT1ΔUG* cells (Figures 2F and 2G). To confirm that the UGUG-rich repeats in the *NEAT1_2* isoform are essential for the localization of TDP-43 to paraspeckles, we inserted a stretch of 60 UG-repeats to the 3′ end of endogenous *NEAT1ΔUG* (Figure 2H), which restored the colocalization of TDP-43 with paraspeckles (Figures 2I and 2J). Taken together, our findings indicate that TDP-43 localizes to paraspeckles because of its direct binding to the *NEAT1_2* isoform, which

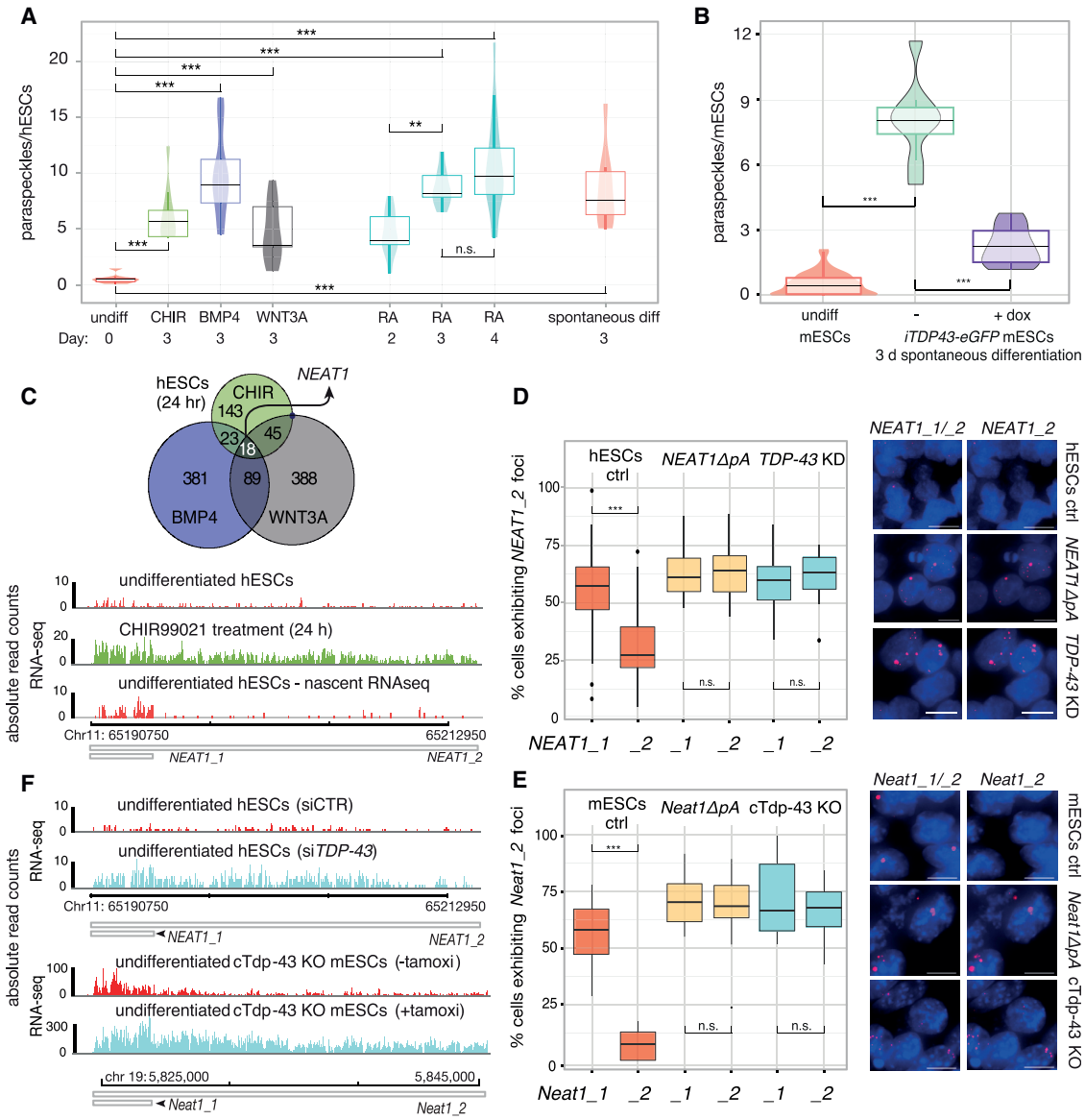

Figure 1. Alternative Polyadenylation of *NEAT1* Induces Paraspeckle Formation upon Differentiation and Depletion of TDP-43 in Mouse and Human ESCs

(A and B) The number of paraspeckles analyzed by counting *NEAT1_1*, *NEAT1_2* (A) or *Neat1_1*, *Neat1_2* (B) double-labeled foci (based on single-molecule fluorescent *in situ* hybridization [smFISH] and criteria explained in Figure S1A).

(A) Undifferentiated hESCs, spontaneously differentiating cells, and BMP4-, CHIR99021-, WNT3A-, and retinoic acid (RA)-treated cells, promoting trophoblast, mesoderm, mesendoderm (primitive streak-like), and neuroectoderm fates, respectively.

(B) Undifferentiated mESCs and spontaneously differentiating *iTDP-43-EGFP* mESCs untreated or treated with doxycycline to ectopically express TDP-43; more than 250 (A) and more than 200 (B) cells analyzed per group, Mann-Whitney *U* test; $^{**}p < 0.001$, $^{***}p < 0.0001$. Duration of treatment was as indicated.

(C) Venn diagram depicting differentially expressed genes in hESCs exposed to the indicated differentiation stimuli for 24 h relative to untreated cells (n = 2 biological replicates of global RNA-seq per condition; adjusted $p < 0.01$, Fisher's exact test, fold change ≥ 4). Bottom: representative mapping of *NEAT1* RNA-seq reads aligned to the two isoforms; global and nascent RNA-seq of undifferentiated hESCs and CHIR99021-treated hESCs (n = 2 biological replicates).

(D and E) Percentage and representative maximum projection photomicrographs of h/mESCs exhibiting *NEAT1_1*, *NEAT1_2* (D) and *Neat1_1*, *Neat1_2* (E) isoforms analyzed as above.

(D) Undifferentiated WT and *NEAT1ΔpA* line and 3-day TDP-43 small interfering RNA (siRNA)-treated hESCs (knockdown [KD]) maintained under pluripotency conditions.

(E) Undifferentiated WT and *Neat1ΔpA* line and cTdp-43 KO (conditional knockout) mESCs 3 days following tamoxifen treatment, which leads to deletion of *Tdp-43* under pluripotency conditions. Statistical analysis and counting as in (A); scale bars, 10 μm. Red, *NEAT1_1*, *_2*, *Neat1_1*, *_2* probes; blue, DAPI (nuclear stain).

(F) Representative mapping of *NEAT1* and *Neat1* RNA-seq reads displaying samples from TDP-43 siRNA KD or control siRNA-treated hESCs (2 days) and untreated or tamoxifen-treated Tdp-43 KO mESCs (2 days, n = 3 biological replicates) under pluripotency conditions.

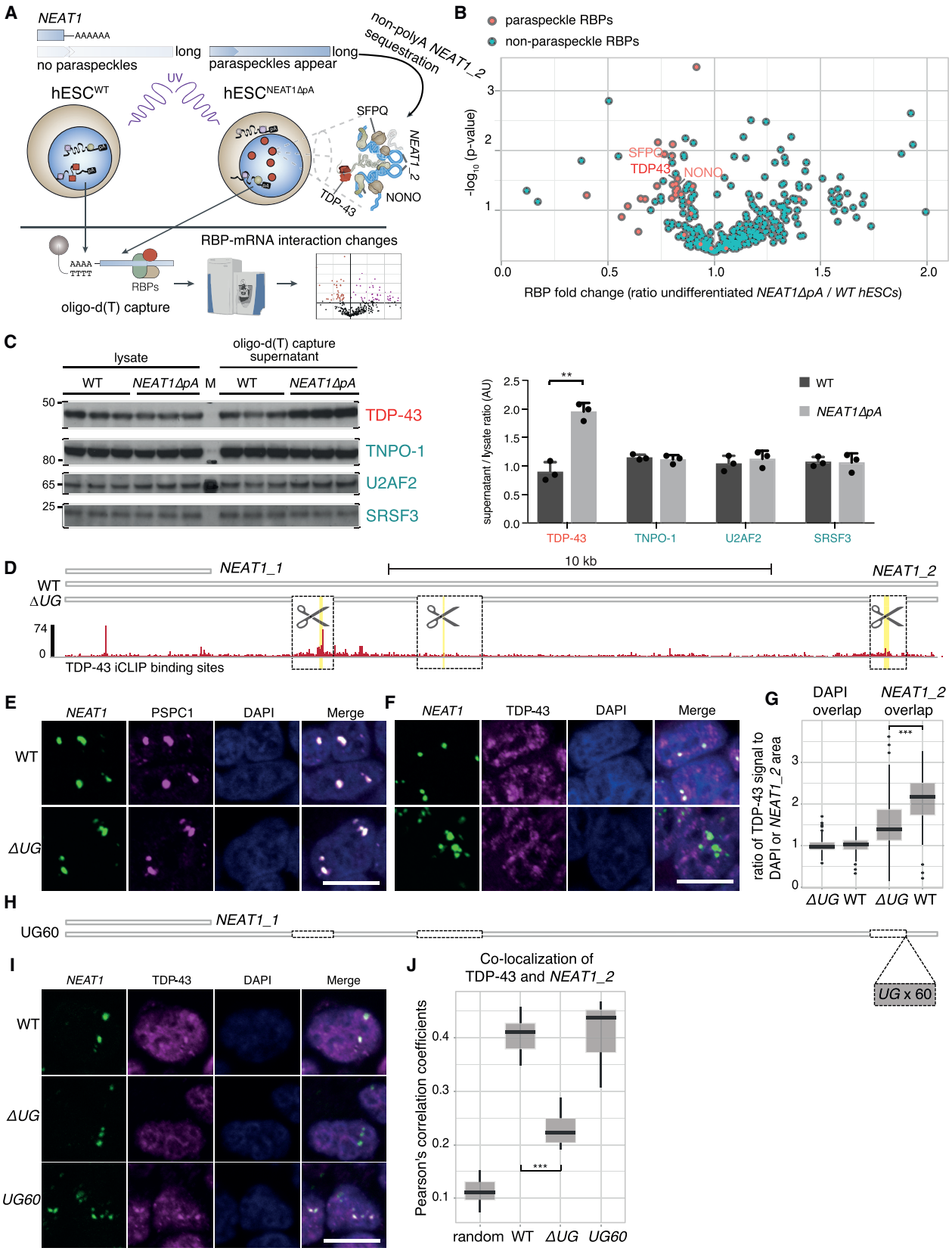

(legend on next page)

partially reduces its binding to polyadenylated RNAs upon paraspeckle formation.

TDP-43 Maintains Pluripotency and Enhances Somatic Cell Reprogramming

The role of TDP-43 in suppressing paraspeckle formation in undifferentiated hESCs or mESCs and TDP-43 sequestration in differentiated cells suggested that it might be regulating pluripotency. To directly examine this, we extracted transcript abundance from 3′ mRNA-seq of conditional *Tdp-43* knockout (cTdp-43 KO) mESCs (Chiang et al., 2010; Figure S2C). This demonstrated that many general pluripotency genes, as defined by a previous study (Kalkan et al., 2017), were significantly downregulated, whereas genes that collectively classify trophectoderm differentiation were upregulated (Figure 3A; Table S3). The only significantly upregulated pluripotency gene was *Lin28a*, but this is consistent with the fact that expression of *Lin28a* increases immediately after the exit from naive pluripotency (Kalkan et al., 2017). Destabilization of pluripotency was also evident by the loss of the dome-shaped compact colony morphology in cTdp-43 KO mESCs (Figure 3B). In contrast, overexpression of TDP-43 promoted pluripotency, as indicated by prolonged expression of SSEA-1 and elevated NANOG upon spontaneous differentiation of mESCs (Figures 3C and 3D).

To analyze this further, we next tested whether overexpression of TDP-43 affects reprogramming of human secondary fibroblasts harboring a doxycycline-inducible OKSM (*OCT4*, *KLF4*, *SOX2*, *C-MYC*) gene cassette (Cacchiarelli et al., 2015; Figure 3E). We found that this results in a nearly 2-fold increase in the number of colonies expressing the pluripotency marker alkaline phosphatase (AP) and a 3-fold increase in cells expressing the pluripotency marker TRA-1-60 (Figures 3F–3I), indicating that TDP-43 facilitates reprogramming. Moreover, transient ectopic expression of TDP-43 during the initial phase of reprogramming of primary adult human fibroblasts led to a 5-fold increase in the number of induced pluripotent stem cell (iPSC) colonies (Figures 3J and 3K).

TDP-43 Regulates APA of Many Transcripts Important for Pluripotency, Including *SOX2*

To further understand the mechanisms whereby TDP-43 promotes pluripotency, we analyzed its global role in pA site selection, which is plausible given our previous findings regarding TDP-43's direct regulation of APA (Rot et al., 2017). We used 3′ mRNA-seq to compare undifferentiated hESCs with mesodermal progenitors that were differentiated by activating the Wnt or β-catenin pathway using a GSK3 inhibitor (Blauwkamp et al., 2012). We confirmed the enrichment of mesoderm gene signature and downregulation of pluripotency genes in the progenitor population by RNA-seq (Figure S3A; Table S4). We also confirmed the validity of the pA sites identified by 3′ mRNA-seq (Figures S3B–S3F). In genes that contained multiple pA sites, we defined the two pA sites with the most significant change between mesodermal progenitors and undifferentiated hESCs. Importantly, we found a correlation between the pA site changes induced by differentiation or by *TDP-43* knockdown (KD) in undifferentiated hESCs (Pearson's correlation coefficient (r) = 0.62; Figure 4A; Table S5). This indicates that the decreased activity of TDP-43 upon early differentiation is a major cause of differentiation-induced APA.

To systematically identify the primary RNA motifs that contribute to the regulation of APA, we analyzed the enriched sequence motifs. We identified GU-rich motifs as the highest-ranking sequences that are enriched around the pA sites that changed during hESC differentiation (Figure S4A). Notably, similar motifs were enriched around differential pA sites affected by KD of *TDP-43* in undifferentiated hESCs and by cTdp-43 KO in mESCs (Figure S4A). Moreover, RNA maps of these motifs showed that they are located in the region upstream of the regulated pA sites (Figures S4B–S4D), where accessory regulatory sites typically reside (Di Giammartino et al., 2011). The similar pattern of motif enrichment for all conditions (Figure S4A) and the high correlation in processing changes upon differentiation or *TDP-43* KD (Figure 4A) indicated that binding of TDP-43 close to the regulated pA sites could explain a large portion of the global changes in APA that take place upon differentiation of hESCs or mESCs.

To validate the direct binding of TDP-43 to the regulated pA sites, we conducted individual nucleotide-resolution UV crosslinking and immunoprecipitation (iCLIP) experiments with TDP-43 in hESCs (König et al., 2010). A direct role of TDP-43 in APA regulation was evident by the clear position-dependent dual enrichment of its binding sites around the pA sites that undergo

Figure 2. *NEAT1_2* Recruits TDP-43 into Paraspeckles

(A) A schematic overview of the mRNA-interactome analysis strategy used for identifying relocalized RBPs upon paraspeckle formation. Peptides were identified by UV crosslinking and capturing mRNA-RBP complexes using Oligod(T)25-bound magnetic beads followed by mass spectrometry. Because deletion of the *NEAT1* pA site promotes paraspeckle formation in undifferentiated hESCs (Figure 1), comparing peptide counts in *NEAT1ΔpA* with WT cells detects resulting changes in mRNA-RBP occupancy. Further details regarding global mRNA-interactome analysis are given in Figures S2D–S2F.

(B) A Volcano plot displaying fold changes of mRNA-bound RBPs in *NEAT1ΔpA* undifferentiated hESCs and their respective statistical score (t test, n = 3 biological replicates per condition). Previously identified paraspeckle proteins are labeled red.

(C) Western blot analysis of TDP-43 and non-paraspeckle control RBPs of the lysate versus the supernatant fraction after mRNA depletion by Oligod(T) capture, from UV-crosslinked WT and *NEAT1ΔpA* undifferentiated hESCs. Right: quantification (t test, n = 3, $^{**}p < 0.01$).

(D) The positions of TDP-43 cross-linked sites (red bars) in *NEAT1* that were identified by TDP-43 iCLIP (from Tollervey et al., 2011). The 1∼2-kb deleted regions (black boxes) in the *NEAT1ΔUG* cell line, and the positions of the three longest stretches of UG repeats within the transcript (yellow bars) are indicated.

(E–G) Representative maximum projection photomicrographs from RNA-FISH and immunofluorescence of *NEAT1_2* and the paraspeckle markers PSPC1 (E) and TDP-43 (F) in WT and *NEAT1ΔUG* HAP-1 cells. Blue, DAPI (nuclear stain). Scale bars, 10 μm. (G) shows quantification of the TDP-43 immunofluorescence signal in DAPI and *NEAT1* segmented areas corresponding to nuclei and paraspeckles, respectively. More than 200 cells were analyzed per group; Mann-Whitney *U* test, $^{***}p < 0.0001$. The threshold was set on a ratio of TDP-43/*NEAT1* signal as described in the STAR Methods.

(H) Diagram of *NEAT1* corresponding to (C), with the position of an ectopic stretch of 60 UG repeats.

(I and J) Representative maximum projection photomicrographs from *NEAT1* RNA-FISH and TDP-43 immunofluorescence (I) and analysis of co-localization (J). Cell lines included WT, *NEAT1ΔUG*, and *NEAT1ΔUG+UG60* HAP1 cells. Cell numbers and statistical analysis were as in (F). Scale bars, 10 μm.

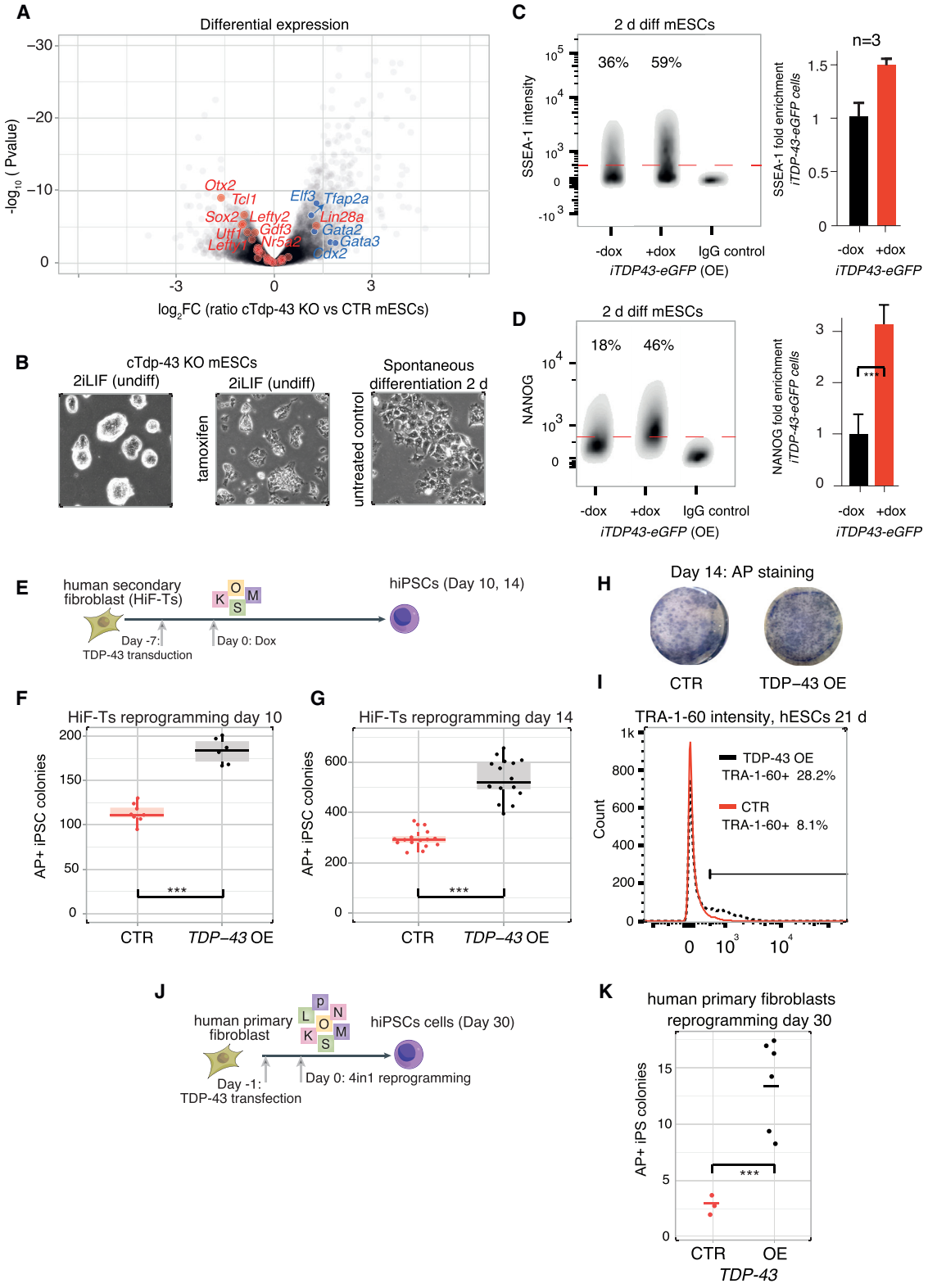

Figure 3. TDP-43 Maintains Pluripotency and Enhances Somatic Cell Reprogramming

(A) Volcano plot displaying gene expression fold changes and their respective statistical score (adjusted p value, Fisher's exact test), comparing untreated and tamoxifen-treated cTdp-43 KO undifferentiated mESCs (n = 10 biological replicates per condition). Known pluripotency and trophectoderm markers are labeled red and blue, respectively (marked factors fulfilled $p < 0.01$).

(legend continued on next page)

APA following *TDP-43* KD or KO, as evident by the RNA map showing the density of its crosslinking in hESCs (Figures S5A–S5E) or of GU-rich motifs (Figures S5F and S5G), consistent with the previously reported RNA map in HEK293 cells (Rot et al., 2017). Enriched binding of TDP-43 was detected close to repressed pA sites (within 100 nt) and further upstream and downstream of enhanced sites (Figure S5F) in a pattern that was also conserved in mESCs (Figure S5G). Notably, TDP-43-dependent regulation of over 40% of the affected pA sites was conserved between hESCs and mESCs (Table S5). These analyses validated the high quality and positional precision of our data and identified the RNA targets that are directly regulated by TDP-43 according to position-dependent principles.

Notably, transcripts exhibiting APA upon cTdp-43 KO were significantly enriched for the GO-term "stem cell maintenance" (Figure 4B; Table S5). Moreover, TDP-43 dictated the APA pattern of the core naive pluripotency network, including *Sox2*, *Nr5a2*, *Esrrb*, *Klf2*, *Tfcp2l1*, *Tbx3*, *Zfp281*, *Tcf7l1*, *Zic3*, and *Tdgf1* (Kalkan et al., 2017), which all changed in the same direction as upon early differentiation (Figure 4C; Figure S3F). One of the conserved APA events was evident in the mRNA encoding the pioneer pluripotency transcription factor *Sox2*. This gene encodes a 3′ UTR harboring two pA sites, and the transcripts showed a proximal-to-distal shift upon *TDP-43* KD in hESCs and cTdp-43 KO in mESCs and upon hESC differentiation (Figure 4D; Table S5). The TDP-43 crosslinking pattern on the *Sox2* transcript in undifferentiated mESCs, in the 100-nt region adjacent to the distal pA site and between 100–200 nt from the proximal site (Figure 4E), is in agreement with the mode of regulation observed by the RNA map analysis (Figure S5G). Furthermore, TDP-43 expression correlated with the abundance of SOX2 protein, which dramatically declined following cTdp-43 KO in mESCs (Figure 4F).

To understand how TDP-43 promotes SOX2 expression, we created a minigene reporter containing the 3′ UTR of *SOX2* located downstream of *EGFP* (Figure 4G). Flow cytometry showed that overexpression of TDP-43 in HEK293T cells increased the GFP signal in the presence of *miR-21*, which could target the long isoform of *SOX2* (Figure 4H). Mutating the proximal pA site in the *SOX2* 3′ UTR made it insensitive to TDP-43, confirming that TDP-43 regulates *SOX2* expression through APA (Figure 4I). Finally, mutating the *miR-21* binding site in the reporter construct, which resides in the long isoform, ablated the effect of TDP-43 on EGFP expression (Figure 4J). Importantly, upregulation of *miR-21* took place upon primitive streak differentiation (Figure 4K), which agrees with the finding that deletion of its binding site in *Sox2* by genome editing led to a dramatic induction of *Sox2* in primitive streak progenitors (Figure 4L). These results show that TDP-43 promotes pluripotency by APA-mediated regulation of pluripotency factors, including *Sox2*.

TDP-43 Represses Formation of Paraspeckles by Regulating APA of *NEAT1*

Beyond direct regulation of pluripotency genes via APA, we sought to understand how TDP-43 regulates paraspeckle formation via APA of *NEAT1*. Given that the *NEAT1* isoform switch takes place upon differentiation and KD of TDP-43 (Figure 1), we speculated that downregulation of TDP-43 coincides with and, therefore, contributes to the isoform switch during differentiation. Indeed, decreased expression of TDP-43 was evident in a published RNA-seq dataset of hESCs differentiated into developmental progenitors (Gifford et al., 2013), which was inverse to the upregulation of *NEAT1_2* (Figure 5A). Moreover, we observed significantly lower levels of TDP-43 transcript and protein upon 3 days of differentiation (Figures 5B and 5C; Figure S5H). Similarly, the expression of *NEAT1* was inversely correlated with pluripotency genes and *TDP-43* during the reprogramming of human fibroblasts to iPSCs (Figure S5I).

To decipher whether TDP-43 directly regulates *NEAT1* processing, we analyzed the RNA-binding profile of TDP-43 by iCLIP (Figures S5A–S5G). This showed that TDP-43 binds to evolutionarily conserved clusters of GU-rich motifs upstream of the pA signal in mESCs (Figure 5D). This pattern agrees with the enhancing effect of TDP-43 when binding more than 100 bp upstream of the pA site in *Sox2* (Figure 4E). To validate the direct effect, we used CRISPR-Cas9 editing of mESCs to excise a 100-nt GU-rich binding site of TDP-43 that is located 105 nt upstream of the internal *Neat1* pA site (Figure 5E; *Neat1Δ100nt* mESCs). Importantly, undifferentiated *Neat1Δ100nt* mESCs exhibited high expression of the *Neat1_2* isoform (Figure 5F) and paraspeckles (Figure 5G), which were induced to a comparable amount as in cTdp-43 KO or *Neat1ΔpA* mESCs. Moreover, we removed growth factors promoting pluripotency from *Neat1Δ100nt* and control mESC cultures to induce paraspeckles while also ectopically expressing *iTDP-43-EGFP*. The capacity of TDP-43-EGFP to repress the expression of *Neat1_2* under these conditions was reduced 2-fold in *Neat1Δ100nt* cells (Figure S5J). Finally, *Neat1Δ100nt* mESCs exhibited an increased differentiation propensity, as evident by the decline of NANOG during spontaneous differentiation (Figure S5K). We concluded that TDP-43 binding upstream of the *Neat1* pA site enhances the production of

(B) Representative photomicrographs of untreated cTdp-43 KO mESCs, following tamoxifen treatment in 2iLIF medium and following 2-day spontaneous differentiation.

(C and D) Representative flow cytometry analyses of spontaneously differentiating (2 days) *iTDP-43-EGFP* mESCs that were treated with doxycycline (overexpression [OE]) or left untreated and immunostained for SSEA-1 (C) and NANOG (D). Non-treated cells were used for immunoglobulin G (IgG) control staining. The mean of three independent experiments is depicted on the right (error bars, SD); two-sided t test, ***$p < 0.001$.

(E–I) Reprogramming of hiF-T secondary fibroblasts with or without (empty vector) transduction of TDP-43, cells harboring doxycycline-inducible reprogramming factors (Cacchiarelli et al., 2015) (E), number of alkaline phosphatase (AP)-positive human induced pluripotent stem cell (hiPSC) colonies emerging on day 10 and 14 of reprogramming (F and G; dots represent replicates from three independent experiments, Mann-Whitney *U* test, ***$p < 0.001$), representative photomicrographs (H), and TRA-1-60 flow cytometry analysis (I); n = 3 independent experiments, gating was based on an IgG control.

(J and K) Reprogramming of primary human fibroblasts (J) and the number of AP-positive colonies on day 30 (dots represent replicates from three independent experiments) with or without (empty vector) transfection of TDP-43 (K); statistical analysis as in (F) and (G).

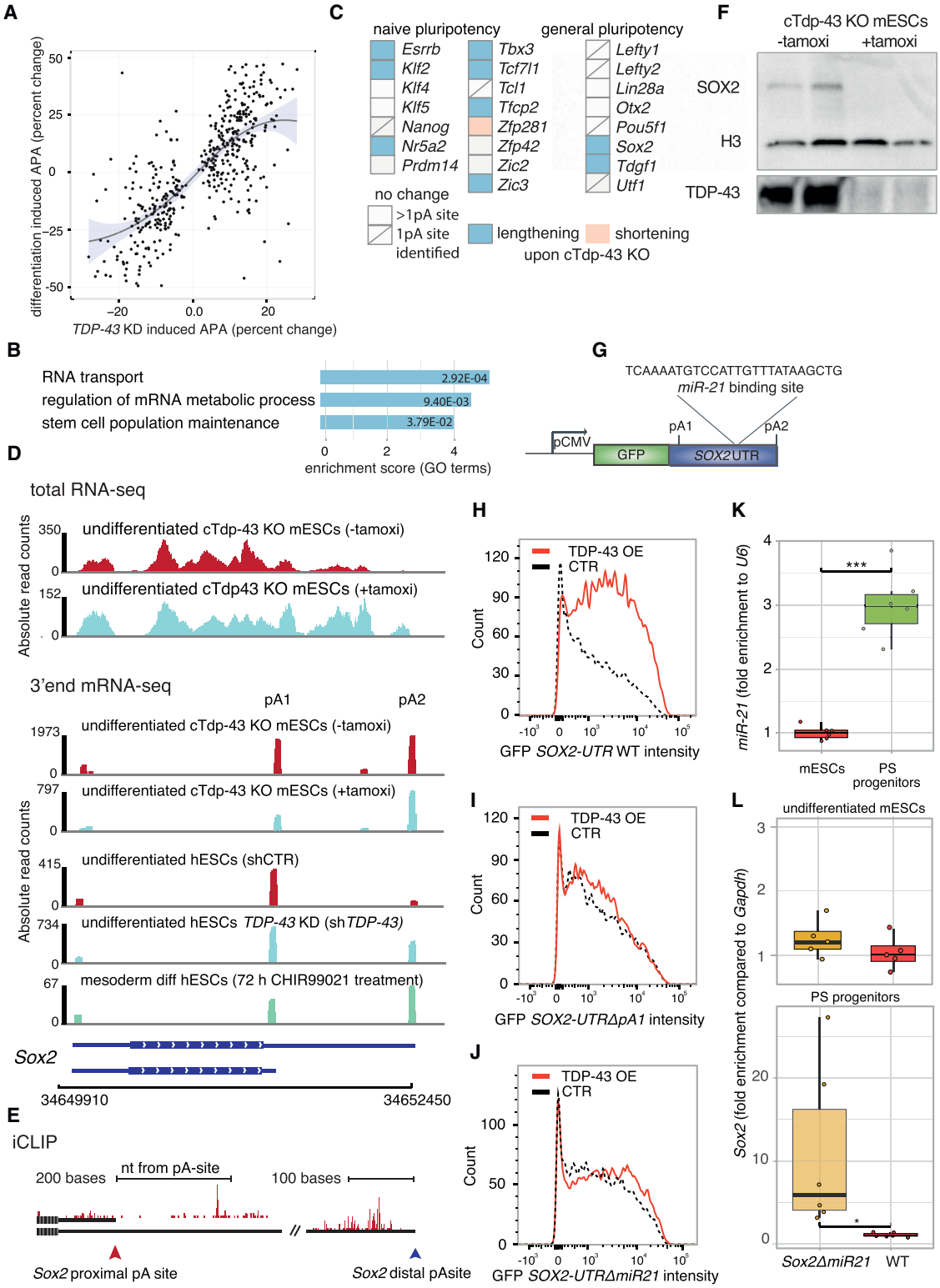

Figure 4. TDP-43 Regulates APA of Genes Important for Pluripotency, Including *Sox2*

(A) Scatterplot displaying relative changes of pA sites upon differentiation of hESCs (Figures S3A and S3B) and changes accruing by knocking down *TDP-43* in undifferentiated hESCs for 48 h (n = 4 control short hairpin [shCTRL] and n = 8 sh*TDP-43* using 2 *TDP-43*-targeting short hairpin RNAs [shRNAs] with 4 replicates for each; adjusted $p < 0.05$, Fisher's exact test). Linear regression (gray line) and the 90% confidence interval region (light blue) are shown (Pearson's correlation

(legend continued on next page)

polyadenylated *Neat1_1*, which decreases the production of *Neat1_2* and assembly of paraspeckles upon differentiation.

Neat1_2 Is Required for Efficient Early Differentiation by Cross-Regulation with TDP-43

To analyze whether *Neat1* functionally regulates the differentiation of ESCs, we excised the triple helix (TH) region at the 3′ end of the gene, which is required for stabilizing *Neat1_2* in somatic cells (Wilusz et al., 2012; Yamazaki et al., 2018). Homozygous TH deletions in mESCs significantly reduced the number of paraspeckles in differentiated cells (Figure 6A; Figure S6A). Notably, the *in vitro* pluripotency phenotype of *Neat1ΔTH* mESCs was significantly prolonged during differentiation, as evident by higher expression of the pluripotency markers SSEA-1 and NANOG (Figures 6B and 6C), mimicking the phenotype of TDP-43 overexpression (Figures 3C and 3D).

To further assess the function of *Neat1_2* during embryonic development, we used tetraploid (4n) mouse embryo ↔ 2n mESC aggregations for generating chimera embryos exclusively derived from mESCs, whereas extra-embryonic lineages were derived from the 4n cells (Figure 6D; Eakin and Hadjantonakis, 2006). We aggregated 4n membrane-targeted, tdTomato-expressing, 2- to 4-cell-stage embryos with wild-type (WT), *Neat1ΔpA*, or *Neat1ΔTH* mESCs, which we generated by editing IDG3.2 mESCs, a line that is routinely used for generating full-term chimeras (Engert et al., 2013). Embryonic day 7.75 (E7.75) to E8.0 embryos derived from *Neat1ΔTH* mESCs were abnormal and exhibited defective patterning of axial mesoderm and the node, as indicated by scattered expression of FOXA2 and BRACHYURY (Figures 6E and 6F; Figures S6B and S6C). Scattered expression of FOXA2 also suggested that the identity of definitive and visceral endoderm was perturbed (Figure S6C).

In contrast, we did not observe morphological abnormalities of chimera embryos derived from *Neat1ΔpA* or WT mESCs (Figures 6E and 6F; Figures S6D and S6E), which efficiently form paraspeckles (Figure 1D). We also looked for phenotypic effects of inducing *NEAT1_2* in undifferentiated, pluripotent *NEAT1ΔpA* hESCs. Comparison with the parental cells showed that a cohort of mesoderm and endoderm markers were already expressed in the undifferentiated state, plausibly in subpopulations, despite the cells being maintained in pluripotency conditions (Figure S6F). Taken together, these results demonstrate that paraspeckle formation facilitates the differentiation of pluripotent cells and embryonic patterning.

Last, we analyzed the interdependence of TDP-43 and *Neat1_2* in the regulation of early spontaneous differentiation. We manipulated the two factors concomitantly by deleting the endogenous TH region in *Neat1_2* in the *cTdp-43* KO mESC line. Paraspeckles are normally increased upon inducible KO of *Tdp-43* by tamoxifen treatment of cTdp-43 KO mESCs (Figure 1E), whereas *Neat1ΔTH* mESCs are defective in the induction of paraspeckles (Figure 6A; Figure S6A). We assessed whether deficient induction of paraspeckles upon tamoxifen treatment of the cTdp-43 KO *Neat1ΔTH* mESCs affects any of the cellular responses to TDP-43 depletion. Indeed, the key pluripotency proteins SOX2 and NANOG were downregulated to a lesser extent upon spontaneous differentiation and tamoxifen treatment of cTdp-43 KO *Neat1ΔTH* mESCs with deficient paraspeckle induction compared with cTdp-43KO mESCs Figures 6G–6J). Global transcriptome analysis revealed the same trend, evident by maintained expression of pluripotency genes and reduced expression of early differentiation genes, including *Cdx2* and *Brachyury* (Figure 6K; Table S6). This was supported by the higher proliferative capacity of tamoxifen-treated differentiating cTdp-43 KO *Neat1ΔTH* mESCs compared with *Neat1* WT mESCs (Figure 6L). Strikingly, we observed a dramatic reduction in the number of APA-regulated genes in tamoxifen-treated cTdp-43KO *Neat1ΔTH* mESCs as compared with control cells where induction of cTdp-43KO induces paraspeckles (Figure 6M; Table S6). Thus, decreased abundance of TDP-43 promotes dissolution of pluripotency largely through APA regulation, but induction of *Neat1_2* is required for efficient APA regulation. Collectively, we conclude that cross-regulation between *Neat1* and TDP-43 is essential for their efficient reciprocal roles in the pluripotency-differentiation transition.

coefficient [r] = 0.62). Increased use of the proximal pA site has positive values, and decreased use has negative values, based on genes passing filtering and statistical analysis as outlined in Figures S3C–S3E.

(B and C) Non-redundant Gene Ontology (GO) terms (B) and ground-state and general pluripotency factors (C), characterized by (Kalkan et al., 2017), of genes exhibiting APA upon cTdp-43 KO in mESCs (n = 10 independent sample replicates per group; genes passing filtering and statistical analysis as outlined in Figure S3C–S3E).

(D) Representative diagrams displaying the transcript isoforms of *Sox2* upon cTdp-43 KO in mESCs and frequencies of the pA sites in *Sox2* and *SOX2* upon cTdp-43 KO in mESCs or KD of TDP-43 and 72 h CHIR99021 treatment of hESCs; samples as above.

(E) The positions of TDP-43 crosslinking (red bars) in *Sox2* transcript from mESCs, as defined by iCLIP, surrounding the proximal and distal pA sites; n = 2 biological replicates (Figure S5C) combined into a single track.

(F) Western blot analysis of SOX2, TDP-43, and histone H3 following tamoxifen treatment (3 days) of cTdp-43 KO mESCs; independent replicates are shown.

(G) An illustration of the *EGFP-SOX2* 3′ UTR reporter minigene displaying endogenous positions of the proximal and distal pA sites and the *miR-21* binding site.

(H–J) Representative flow cytometry analyses of HEK293T cells with the doxycycline-inducible TDP-43 gene cassette co-transfected with *miR-21* (transfected cells were gated using tdTomato as described in STAR Methods), and the respective *EGFP-SOX2* 3′ UTR constructs: unmodified (H), harboring deletion of the proximal pA site (I), or with deletion of the *miR-21* binding site (J). Control (CTR) indicates cells that were not treated with doxycycline.

(K) Boxplot depicting relative levels of *miR-21* in undifferentiated mESCs and in primitive streak (PS)-like progenitors generated by 3 d CHIR99021 treatment (n = 6 independent replicates, two sided t test; p value *** $\leq$ 0.001).

(L) Boxplot analyses depicting levels of the *Sox2* transcript in WT mESCs and cells lacking the endogenous *miR-21* binding site in *Sox2* (*Sox2ΔmiR21*) under pluripotency conditions (top) and upon PS differentiation (bottom) (n = 5 and 6 independent replicates, two-sided t test; *p $\leq$ 0.01).

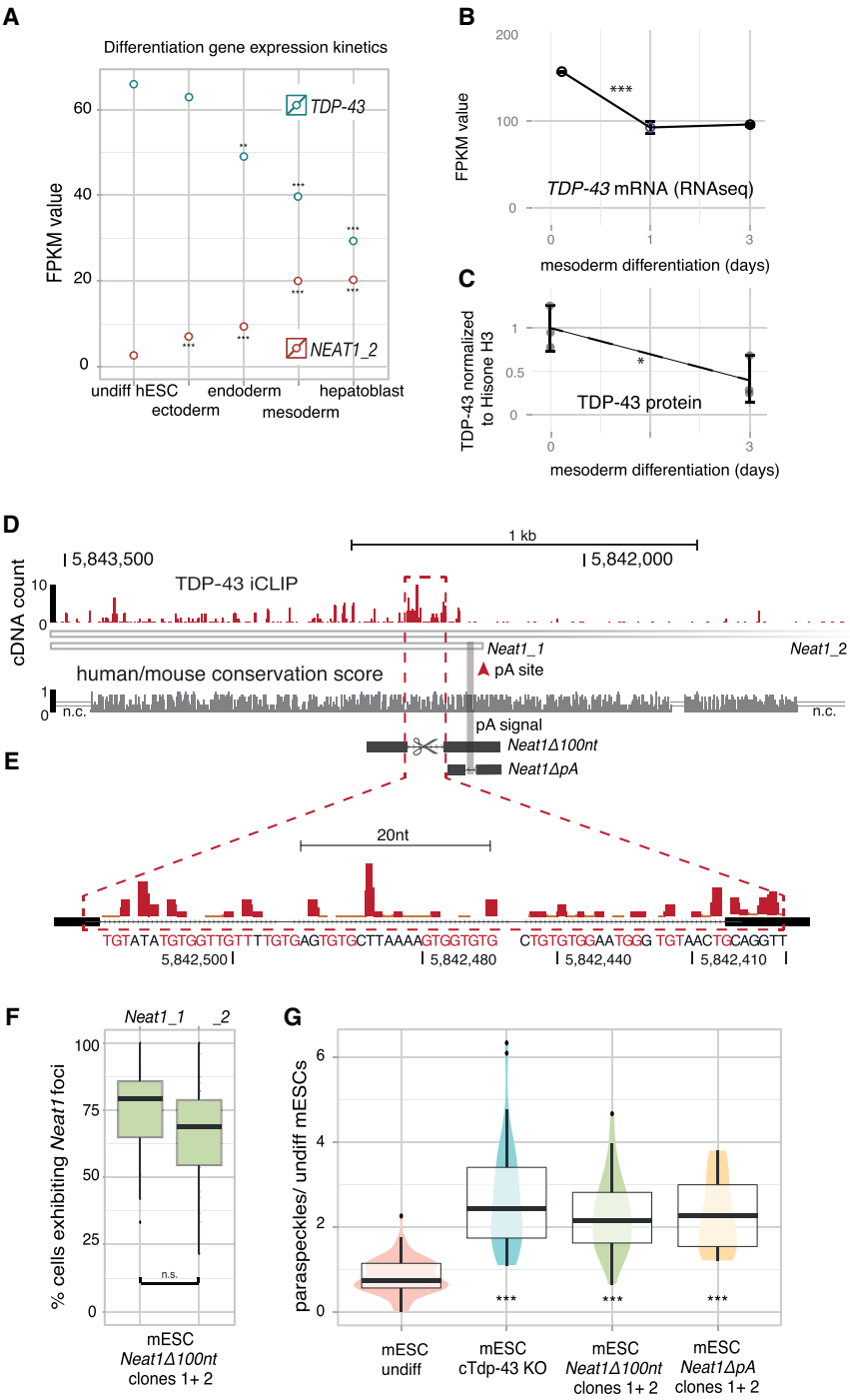

Figure 5. TDP-43 Directly Promotes *Neat1* Polyadenylation to Repress Paraspeckles in Pluripotent Cells

(A) Normalized expression of *TDP-43* and *NEAT1* in undifferentiated hESCs and differentiated developmental progenitors (transcriptome data from Gifford et al., 2013).

(B and C) Quantification of TDP-43 during hESC differentiation, the transcript (B) based on Figure 1C, and on western blotting (C) using histone H3 for normalization (representative blot in Figure S5H). Samples were derived from undifferentiated hESCs and cells differentiated toward mesoderm progenitors using CHIR99021; (B) Fisher's exact test and n = 2 and (C) t test, n = 3 independent replicates, as indicated by dots; error bars, SD; *p ≤ 0.05, ***p ≤ 0.001).

(D) TDP-43 crosslinked positions (red bars) in the *Neat1* transcript (shown are *Neat1_1* and the 5′ region of *Neat1_2*) from mESCs analyzed by iCLIP (replicates and samples as in Figure 4E). Sequence conservation score is plotted as gray bars (n.c., not conserved).

(E) Modified mESC lines lacking the endogenous binding site of TDP-43 upstream of the pA site (*Neat1Δ100nt*) or lacking the pA signal (*Neat1ΔpA*). The region deleted in the *Neat1Δ100* mESC line is highlighted and enlarged, showing the GU-rich motifs and the TDP-43 crosslinking positions in the region (based on D).

(F and G) Percentage of cells exhibiting *Neat1_1* or *Neat1_2* foci (F) and number of paraspeckles in undifferentiated mESCs lines (G) and parental WT, *Neat1Δ100nt*, cTdp-43 KO mESC line 2 days following tamoxifen treatment and *Neat1ΔpA* (cell numbers analyzed, replicates, and statistical analysis as in Figure 1B).

DISCUSSION

Network modules that promote efficient cell state transitions are inherent to differentiation, regulation of organismal development, homeostasis, and regeneration (Alon, 2007). Cross-regulation between regulatory factors can promote lineage bifurcation and has been associated with transcription factors, microRNAs, and signaling cascades (Alon, 2007; Enver et al., 2009; Rybak et al., 2008). We show here that cross-regulation between paraspeckles and TDP-43 is similarly essential for their efficient roles in promoting transition between pluripotent and differentiated cell fates. TDP-43 inhibits differentiation of ESCs, and lowers the barrier for somatic cell reprogramming, but its abundance decreases during exit from pluripotency, which changes APA of hundreds of genes, including the lncRNA *Neat1* to induce the *Neat1_2* isoform. As a result, TDP-43 is recruited into paraspeckles, which partially sequester it away from mRNAs, further decreasing the activity of TDP-43 in regulating APA during early differentiation. Induction of *Neat1_2* is essential for efficient early differentiation of ESCs and embryonic patterning during gastrulation. Thus, cross-regulation between TDP-43 and paraspeckles is reflected in the reciprocal biological functions of these two factors in promoting either the pluripotent state or differentiation of ESCs.

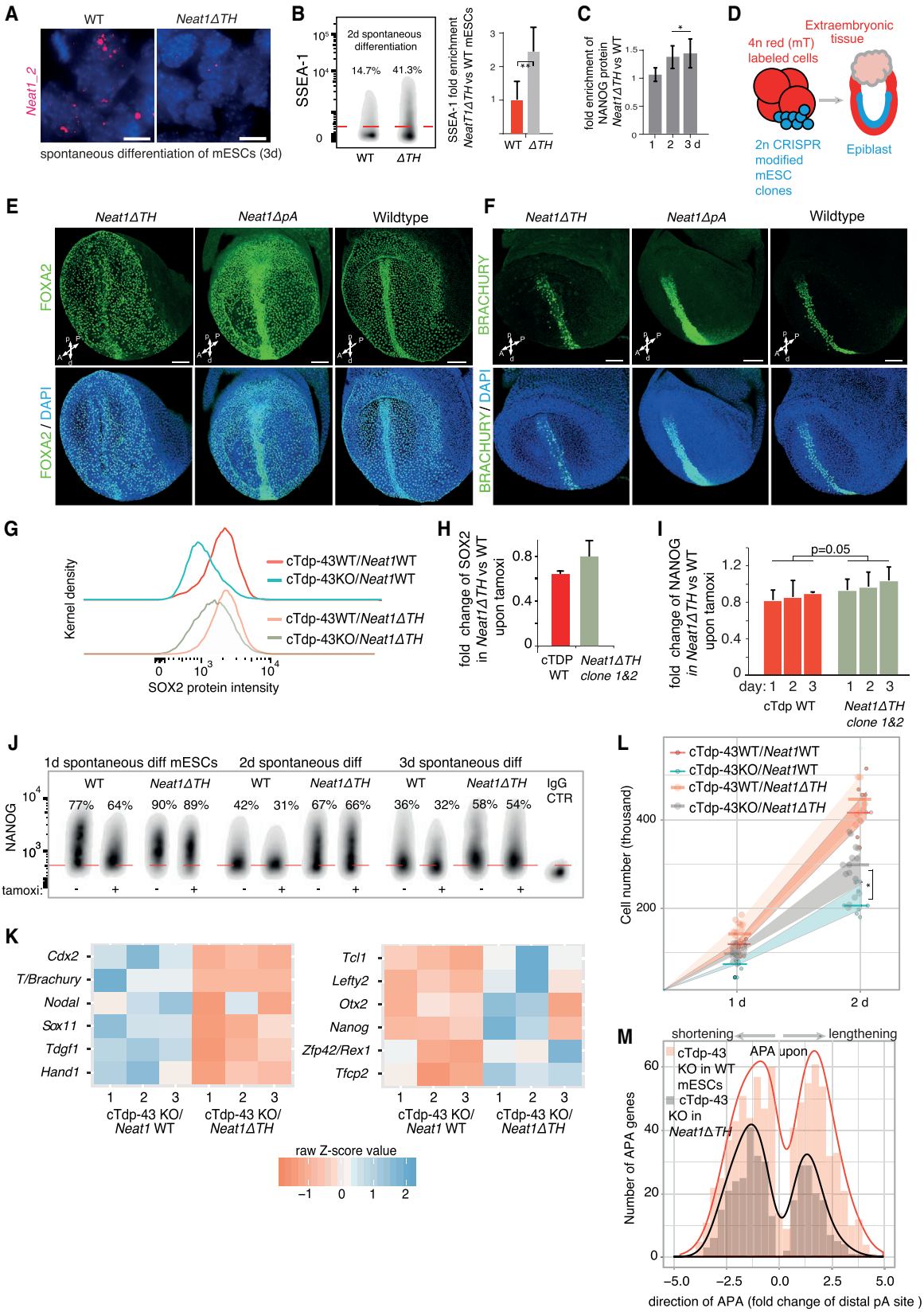

(legend on next page)

Changes in APA have been observed previously during differentiation processes that include myogenesis, adipogenesis, and embryogenesis (Di Giammartino et al., 2011; Hoque et al., 2013). Moreover, the core elements of the cleavage and polyadenylation complex, FIP1 (Lackford et al., 2014) and NUDT21 (Brumbaugh et al., 2018) have been implicated in the regulation of APA during ESC differentiation. Here we used iCLIP and motif analysis to show how TDP-43 regulates APA of specific transcripts through binding to RNA motifs around the regulated pA sites (Figures S4 and S5). Therefore, TDP-43 has a conserved role in promoting the production of short *Sox2* transcript, which is required for efficient expression of this pluripotency and reprogramming factor. It also promotes the short isoform of *Neat1_1*, which suppresses paraspeckle formation. This role of TDP-43 in early cell fate transitions is in line with the past observation that it is essential for murine development (Sephton et al., 2010).

When the pendulum swings in the direction of differentiation, the abundance of TDP-43 decreases to a level permissive for an isoform switch in *NEAT1*, resulting in the production of *NEAT1_2* that scaffolds paraspeckles. It has been shown previously that efficient interaction of TDP-43 and several other RBPs with *NEAT1_2* occurs as a result of phase separation into paraspeckles (Maharana et al., 2018; Yamazaki et al., 2018). Here we have shown that induction of *NEAT1_2* in ESCs partly sequesters TDP-43 and other paraspeckle RBPs away from mRNAs, most likely because of their recruitment into the paraspeckle compartment. This sequestration could contribute to the decreased activity of TDP-43 upon early differentiation, facilitating the global shift in APA and, therefore, exit from pluripotency, which could partly explain how *Neat1_2* promotes early differentiation. It is likely that *Neat1* also acts through additional mechanisms, such as the recently reported role of *NEAT1_2* in scaffolding microprocessor and other RBPs into paraspeckles to regulate microRNA biogenesis (Jiang et al., 2017), and *Neat1_1* on its own could form "microspeckles," whose functions are currently unknown (Li et al., 2017). Thus, our study indicates that formation of a membraneless compartment can be regulated through the processing of its RNA scaffold to coordinate a specific developmental transition.

We have characterized developmental phenotypes of embryonic cells lacking the TH of *Neat1*, which have a reduced number of paraspeckles because of destabilized *Neat1_2*. We used the tetraploid complementation approach, which normally generates viable embryos from ESCs and is used to investigate the role of factors of interest in embryonic tissues (Eakin and Hadjantonakis, 2006). This method enables classifications of embryonic versus extraembryonic phenotypes by circumventing pre-blastocyst developmental arrest, which has been observed upon depletion of *Neat1_2* in a recent study (Hupalowska et al., 2018). Tetraploid complemented embryos derived from *Neat1ΔTH* mESCs have inefficient patterning during gastrulation. Notably, we observed elevated expression of the transcription factor *Cdx2* as the major change that distinguishes the response of *Neat1ΔTH* and WT mESCs to loss of TDP-43 (Figure 6K), which agrees with the previously observed role of *Neat1* in regulating *Cdx2* (Hupalowska et al., 2018). The findings of both studies are also consistent with previous studies that observed decreased litter size, aberrant mammary gland morphogenesis, and smaller pups (Nakagawa et al., 2014; Standaert et al., 2014) in *Neat1* KO mice, which lack paraspeckles (Nakagawa et al., 2011). This phenotype of *Neat1* KO mice is surprisingly mild, given the apparent phenotypes observed in the study, which indicates that the function of *Neat1* might be compensated by additional factors that assist cell fate transitions during *in vivo* murine development.

Beyond the mechanisms of early development, our findings are likely also relevant also for other types of cell fate transitions because both TDP-43 and *NEAT1* are broadly expressed (Shelkovnikova et al., 2018). Moreover, amyotrophic lateral sclerosis (ALS)-causing mutations in TDP-43 affect its phase separation

Figure 6. Efficient Dissolution of Pluripotency upon Depletion of TDP-43 Requires Paraspeckles

(A) Representative photomicrographs demonstrating the downregulation of *Neat1_2* paraspeckles in spontaneously differentiating mESCs by deletion of the triple helix (*ΔTH*) in the 3′ region (further results in Figure S6A). Red, *Neat1_1* and_2 probes; blue, DAPI (nuclear stain). Scale bars, 10 μm.

(B and C) Pluripotency assessment by SSEA-1 (B, right, quantified gated positive cells) and intracellular NANOG (C) flow cytometry of spontaneously differentiating *Neat1ΔTH* and WT mESCs (duration indicated). IgG-treated samples were used for gating positive cells (red line in B). Error bars, SD; two-sided t test; biological replicates, n = 3 per time point; *$p < 0.05$, **$p < 0.01$.

(D–F) *In vivo* analysis of the developmental potency of mESCs exhibiting downregulation of paraspeckles using a 2n mESC - 4n aggregated mouse embryo complementation assay, giving rise, respectively and exclusively, to embryonic and extraembryonic tissues (D). Shown are mouse embryos (E7.75–E8.0) resulting from aggregations of *Neat1ΔTH* and *Neat1ΔpA* mESCs with 4n 2- to 4-cell-stage embryos and representative analysis of FOXA2 (E) and BRACHYURY (F) by immunostaining (n = 7 for *Neat1ΔTH* [5 are shown in Figures S6B and S6C], n = 7 for *Neat1ΔpA* [2 are shown in Figure S6D], and n = 3 for parental control mESC [2 are shown in Figure S6E]). Non-manipulated embryos are shown on the right. Blue, DAPI (nuclear stain). Scale bars, 100 μm. A, anterior; P, posterior; p, proximal; d, distal.

(G–L) Pluripotency assessment by intracellular immunostaining flow cytometry (G–J; error bars, SD, two-sided t test in I, n = 3), RNA-seq (K; n = 3/group, Fisher's exact test), and growth kinetics (L; Mann-Whitney *U* test, $n \geq 8$/group as indicated by dots) in differentiating parental cTdp-43 KO mESCs or the same line harboring *Neat1ΔTH*, treated with tamoxifen during 2.5 days of spontaneous differentiation or left untreated (all consisting of independent replicates). Also shown are representative flow cytometry plots of SOX2 (G) and quantification of gated positive cells according to the IgG control (H) and of NANOG (I and J). IgG-treated samples were used to gate the positive cells (dotted red line) and to quantify the enrichment of these cells. In (K), shown are up- and downregulated representative differentiation and pluripotency genes according to the ScoreCard panel (Tsankov et al., 2015, and Kalkan et al., 2017, respectively), comparing the impact of Tdp-43 KO in mESCs lacking *Neat1_2* (*Neat1ΔTH*) with control mESCs harboring WT *Neat1*. In (L), the width of colored intervals represents the interquartile range of the growth kinetics measurements.

(M) Histogram depicting rearrangements (direction and degree) of pA sites following cTdp-43 KO in *Neat1ΔTH* mESCs compared with the respective parental WT cells (genes passing filtering and statistical analysis as outlined in Figures S3C–S3E; APA in the range of ±5-fold change, $p < 0.01$). mESCs were treated with tamoxifen for 2.5 days or left untreated during spontaneous differentiation (n = 3 independent replicates/group).

properties (Conicella et al., 2016), which could affect its localization into paraspeckles (Yamazaki et al., 2018). Moreover, increased formation of paraspeckles has been observed in motor neurons of patients with ALS (Nishimoto et al., 2013). Therefore, cross-regulation of TDP-43 and *NEAT1* could play a role not just in development but also in diseases such as ALS and cancer, where abnormal RNA granules involving TDP-43 and *NEAT1* are a common feature (Adriaens et al., 2016; Hennig et al., 2015; Nishimoto et al., 2013; Tollervey et al., 2011).

STAR★METHODS

Detailed methods are provided in the online version of this paper and include the following:

- KEY RESOURCES TABLE
- CONTACT FOR REAGENT AND RESOURCE SHARING
- EXPERIMENTAL MODEL AND SUBJECT DETAILS
  - Cell culture
  - Generation of h/mESC lines harboring edited NEAT1/Neat1
  - Generation of HAP-1 cells harboring edited NEAT1
  - Overexpression of TDP-43
  - Knockdown of TDP-43
  - Plasmids
  - Reprogramming of human fibroblasts
  - ANIMALS
- METHOD DETAILS
  - RNA preparation and qRT-PCR assays
  - RNA sequencing
  - Western blotting
  - Immunofluorescence
  - Flow cytometry
  - Subcellular fractionation of hESCs
- QUANTIFICATION AND STATISTICAL ANALYSIS
  - Single molecule (sm)FISH and paraspeckle quantification
  - RNA-FISH and immunofluorescence
  - iCLIP protocol and its analysis
  - RNA-Seq differential expression
  - Identification of polyA sites
  - Analysis of alternative polyadenylation (APA)
  - Visualizing position-dependent polyA site regulation using RNA-maps
  - mRNA/RBP occupancy (mRNA interactome capture)
  - FASP digest
  - Mass spectrometry
  - Analysis of mRNA-interactome
- DATA AND SOFTWARE AVAILABILITY

SUPPLEMENTAL INFORMATION

Supplemental Information can be found online at https://doi.org/10.1016/j.molcel.2019.03.041.

ACKNOWLEDGMENTS

The authors would like to thank Alfredo Castello and Rickie Patani for critical reading of the manuscript. For generous reagent gifts, we are grateful to Derk ten Berge, Philip C. Wong, Shinichi Nakagawa, Michael Kyba, Dieter Edbauer, and Bettina Schmidt. We would like to thank to Anna Pertek and Tajda Klobučar for technical assistance. We are grateful to Nejc Haberman for sequence motif identification, Igor Ruiz de los Mozos for iCount analysis, and Michael Ziller and Joel Ryan for methodological advice. This work was supported by the European Research Council (206726-CLIP and 617837-Translate to J.U.), Slovenian Research Agency (P4-0127, JS-6789, J3-8201, and J3-9263 to B.R.), an IMPRS Max Planck Society fellowship (to M.M.), the Francis Crick Institute, which receives its core funding from Cancer Research UK (FC001002), the UK Medical Research Council (FC001002), and the Wellcome Trust (FC001002), and Seed Funding Award by the UHU Network (UWA, Helmholtz, UCL, to M.D.).

AUTHOR CONTRIBUTIONS

M.M. conceived the study and performed majority of the experiments apart from smFISH, which was carried out and analyzed by M.G. M.G. also generated modified hESC lines. M.G., E.R., and M.M. performed flow cytometry of genetically edited m/hESC lines. S.S. performed chimera experiments under the supervision of H.L. T.Y. generated ΔUG and UG60 HAP1 lines and performed imaging experiments with them under the supervision of T.H. E.R., T.L., D.C., and A.M. contributed to the reprogramming experiments. F.C.Y.L. and M.M. performed mRNA-RBP occupancy experiments, assisted by M.P., and S.M.H. and J.M.-P. oversaw the MS analysis. D.S. performed nascent RNA-seq. G.R. and M.M. analyzed the data, with contributions from C.v.M. and B.R. M.D. and J.U. jointly supervised the study. M.M., J.U., and M.D. wrote the manuscript.

DECLARATION OF INTERESTS

The authors declare no competing interests.

Received: April 29, 2018
Revised: February 12, 2019
Accepted: March 28, 2019
Published: April 29, 2019

REFERENCES

Adriaens, C., Standaert, L., Barra, J., Latil, M., Verfaillie, A., Kalev, P., Boeckx, B., Wijnhoven, P.W.G., Radaelli, E., Vermi, W., et al. (2016). p53 induces formation of NEAT1 lncRNA-containing paraspeckles that modulate replication stress response and chemosensitivity. Nat. Med. *22*, 861–868.

Akhtar, M.N., Bukhari, S.A., Fazal, Z., Qamar, R., and Shahmuradov, I.A. (2010). POLYAR, a new computer program for prediction of poly(A) sites in human sequences. BMC Genomics *11*, 646.

Alon, U. (2007). An Introduction to Systems Biology: Design Principles of Biological Circuits, Third Edition (Chapman and Hall/CRC).

Baltz, A.G., Munschauer, M., Schwanhäusser, B., Vasile, A., Murakawa, Y., Schueler, M., Youngs, N., Penfold-Brown, D., Drew, K., Milek, M., et al. (2012). The mRNA-bound proteome and its global occupancy profile on protein-coding transcripts. Mol. Cell *46*, 674–690.

Blake, J.A., Christie, K.R., Dolan, M.E., Drabkin, H.J., Hill, D.P., Ni, L., Sitnikov, D., Burgess, S., Buza, T., Gresham, C., et al.; Gene Ontology Consortium (2015). Gene Ontology Consortium: going forward. Nucleic Acids Res. *43*, D1049–D1056.

Blauwkamp, T.A., Nigam, S., Ardehali, R., Weissman, I.L., and Nusse, R. (2012). Endogenous Wnt signalling in human embryonic stem cells generates an equilibrium of distinct lineage-specified progenitors. Nat. Commun. *3*, 1070.

Brumbaugh, J., Di Stefano, B., Wang, X., Borkent, M., Forouzmand, E., Clowers, K.J., Ji, F., Schwarz, B.A., Kalocsay, M., Elledge, S.J., et al. (2018). Nudt21 Controls Cell Fate by Connecting Alternative Polyadenylation to Chromatin Signaling. Cell *172*, 106–120.e21.

Budini, M., Romano, V., Quadri, Z., Buratti, E., and Baralle, F.E. (2015). TDP-43 loss of cellular function through aggregation requires additional structural

determinants beyond its C-terminal Q/N prion-like domain. Hum. Mol. Genet. *24*, 9–20.

Cacchiarelli, D., Trapnell, C., Ziller, M.J., Soumillon, M., Cesana, M., Karnik, R., Donaghey, J., Smith, Z.D., Ratanasirintrawoot, S., Zhang, X., et al. (2015). Integrative Analyses of Human Reprogramming Reveal Dynamic Nature of Induced Pluripotency. Cell *162*, 412–424.

Castello, A., Fischer, B., Eichelbaum, K., Horos, R., Beckmann, B.M., Strein, C., Davey, N.E., Humphreys, D.T., Preiss, T., Steinmetz, L.M., et al. (2012). Insights into RNA biology from an atlas of mammalian mRNA-binding proteins. Cell *149*, 1393–1406.

Castello, A., Horos, R., Strein, C., Fischer, B., Eichelbaum, K., Steinmetz, L.M., Krijgsveld, J., and Hentze, M.W. (2013). System-wide identification of RNA-binding proteins by interactome capture. Nat. Protoc. *8*, 491–500.

Chen, L.-L., and Carmichael, G.G. (2009). Altered nuclear retention of mRNAs containing inverted repeats in human embryonic stem cells: functional role of a nuclear noncoding RNA. Mol. Cell *35*, 467–478.

Chiang, P.M., Ling, J., Jeong, Y.H., Price, D.L., Aja, S.M., and Wong, P.C. (2010). Deletion of TDP-43 down-regulates Tbc1d1, a gene linked to obesity, and alters body fat metabolism. Proc. Natl. Acad. Sci. USA *107*, 16320–16324.

Conicella, A.E., Mittal, J., Fawzi, N.L., Conicella, A.E., Zerze, H., Mittal, J., and Fawzi, N.L. (2016). ALS Mutations Disrupt Phase Separation Mediated by α-Helical Structure in the TDP-43 Low-Complexity C-Terminal Domain. Structure *24*, 1537–1549.

Derti, A., Garrett-Engele, P., Macisaac, K.D., Stevens, R.C., Sriram, S., Chen, R., Rohl, C.A., Johnson, J.M., and Babak, T. (2012). A quantitative atlas of polyadenylation in five mammals. Genome Res. *22*, 1173–1183.

Di Giammartino, D.C., Nishida, K., and Manley, J.L. (2011). Mechanisms and consequences of alternative polyadenylation. Mol. Cell *43*, 853–866.

Dobin, A., Davis, C.A., Schlesinger, F., Drenkow, J., Zaleski, C., Jha, S., Batut, P., Chaisson, M., and Gingeras, T.R. (2013). STAR: ultrafast universal RNA-seq aligner. Bioinformatics *29*, 15–21.

Eakin, G.S., and Hadjantonakis, A.K. (2006). Production of chimeras by aggregation of embryonic stem cells with diploid or tetraploid mouse embryos. Nat. Protoc. *1*, 1145–1153.

Engert, S., Burtscher, I., Liao, W.P., Dulev, S., Schotta, G., and Lickert, H. (2013). Wnt/β-catenin signalling regulates Sox17 expression and is essential for organizer and endoderm formation in the mouse. Development *140*, 3128–3138.

Enver, T., Pera, M., Peterson, C., and Andrews, P.W. (2009). Stem cell states, fates, and the rules of attraction. Cell Stem Cell *4*, 387–397.

Flynn, R.A., and Chang, H.Y. (2014). Long noncoding RNAs in cell-fate programming and reprogramming. Cell Stem Cell *14*, 752–761.

Fox, A.H., Nakagawa, S., Hirose, T., and Bond, C.S. (2018). Paraspeckles: Where Long Noncoding RNA Meets Phase Separation. Trends Biochem. Sci. *43*, 124–135.

Gifford, C.A., Ziller, M.J., Gu, H., Trapnell, C., Donaghey, J., Tsankov, A., Shalek, A.K., Kelley, D.R., Shishkin, A.A., Issner, R., et al. (2013). Transcriptional and epigenetic dynamics during specification of human embryonic stem cells. Cell *153*, 1149–1163.

Hennig, S., Kong, G., Mannen, T., Sadowska, A., Kobelke, S., Blythe, A., Knott, G.J., Iyer, K.S., Ho, D., Newcombe, E.A., et al. (2015). Prion-like domains in RNA binding proteins are essential for building subnuclear paraspeckles. J. Cell Biol. *210*, 529–539.

Hirose, T., Virnicchi, G., Tanigawa, A., Naganuma, T., Li, R., Kimura, H., Yokoi, T., Nakagawa, S., Bénard, M., Fox, A.H., et al. (2014). NEAT1 long noncoding RNA regulates transcription via protein sequestration within subnuclear bodies. Mol. Biol. Cell *25*, 169–183.

Hitz, C., Wurst, W., and Kühn, R. (2007). Conditional brain-specific knockdown of MAPK using Cre/loxP regulated RNA interference. Nucleic Acids Res. *35*, e90.

Hoque, M., Ji, Z., Zheng, D., Luo, W., Li, W., You, B., Park, J.Y., Yehia, G., and Tian, B. (2013). Analysis of alternative cleavage and polyadenylation by 3′ region extraction and deep sequencing. Nat. Methods *10*, 133–139.

Hupalowska, A., Jedrusik, A., Zhu, M., Bedford, M.T., Glover, D.M., and Zernicka-Goetz, M. (2018). CARM1 and paraspeckles regulate pre-implantation mouse embryo development. Cell *175*, 1902–1916.e13.

Huppertz, I., Attig, J., D'Ambrogio, A., Easton, L.E., Sibley, C.R., Sugimoto, Y., Tajnik, M., König, J., and Ule, J. (2014). iCLIP: protein-RNA interactions at nucleotide resolution. Methods *65*, 274–287.

Jiang, L., Shao, C., Wu, Q.J., Chen, G., Zhou, J., Yang, B., Li, H., Gou, L.T., Zhang, Y., Wang, Y., et al. (2017). NEAT1 scaffolds RNA-binding proteins and the Microprocessor to globally enhance pri-miRNA processing. Nat. Struct. Mol. Biol. *24*, 816–824.

Kalkan, T., Olova, N., Roode, M., Mulas, C., Lee, H.J., Nett, I., Marks, H., Walker, R., Stunnenberg, H.G., Lilley, K.S., et al. (2017). Tracking the embryonic stem cell transition from ground state pluripotency. Development *144*, 1221–1234.

Kawaguchi, T., Tanigawa, A., Naganuma, T., Ohkawa, Y., Souquere, S., Pierron, G., and Hirose, T. (2015). SWI/SNF chromatin-remodeling complexes function in noncoding RNA-dependent assembly of nuclear bodies. Proc. Natl. Acad. Sci. USA *112*, 4304–4309.

König, J., Zarnack, K., Rot, G., Curk, T., Kayikci, M., Zupan, B., Turner, D.J., Luscombe, N.M., and Ule, J. (2010). iCLIP reveals the function of hnRNP particles in splicing at individual nucleotide resolution. Nat. Struct. Mol. Biol. *17*, 909–915.

Kyba, M., Perlingeiro, R.C.R., and Daley, G.Q. (2002). HoxB4 confers definitive lymphoid-myeloid engraftment potential on embryonic stem cell and yolk sac hematopoietic progenitors. Cell *109*, 29–37.

Lackford, B., Yao, C., Charles, G.M., Weng, L., Zheng, X., Choi, E.A., Xie, X., Wan, J., Xing, Y., Freudenberg, J.M., et al. (2014). Fip1 regulates mRNA alternative polyadenylation to promote stem cell self-renewal. EMBO J. *33*, 878–889.

Li, R., Harvey, A.R., Hodgetts, S.I., and Fox, A.H. (2017). Functional dissection of NEAT1 using genome editing reveals substantial localization of the NEAT1_1 isoform outside paraspeckles. RNA *23*, 872–881.

Ling, J.P., Pletnikova, O., Troncoso, J.C., and Wong, P.C. (2015). TDP43 repression of nonconserved cryptic exons is compromised in ALS-FTD. Science *349*, 650–655.

Maharana, S., Wang, J., Papadopoulos, D.K., Richter, D., Pozniakovsky, A., Poser, I., Bickle, M., Rizk, S., Guillén-Boixet, J., Franzmann, T.M., et al. (2018). RNA buffers the phase separation behavior of prion-like RNA binding proteins. Science *360*, 918–921.

Mao, Y.S., Sunwoo, H., Zhang, B., and Spector, D.L. (2011). Direct visualization of the co-transcriptional assembly of a nuclear body by noncoding RNAs. Nat. Cell Biol. *13*, 95–101.

Merl, J., Ueffing, M., Hauck, S.M., and von Toerne, C. (2012). Direct comparison of MS-based label-free and SILAC quantitative proteome profiling strategies in primary retinal Müller cells. Proteomics *12*, 1902–1911.

Muzumdar, M.D., Tasic, B., Miyamichi, K., Li, L., and Luo, L. (2007). A global double-fluorescent Cre reporter mouse. Genesis *45*, 593–605.

Naganuma, T., Nakagawa, S., Tanigawa, A., Sasaki, Y.F., Goshima, N., and Hirose, T. (2012). Alternative 3′-end processing of long noncoding RNA initiates construction of nuclear paraspeckles. EMBO J. *31*, 4020–4034.

Nakagawa, S., Naganuma, T., Shioi, G., and Hirose, T. (2011). Paraspeckles are subpopulation-specific nuclear bodies that are not essential in mice. J. Cell Biol. *193*, 31–39.

Nakagawa, S., Shimada, M., Yanaka, K., Mito, M., Arai, T., Takahashi, E., Fujita, Y., Fujimori, T., Standaert, L., Marine, J.-C., and Hirose, T. (2014). The lncRNA Neat1 is required for corpus luteum formation and the establishment of pregnancy in a subpopulation of mice. Development *141*, 4618–4627.

Nishimoto, Y., Nakagawa, S., Hirose, T., Okano, H.J., Takao, M., Shibata, S., Suyama, S., Kuwako, K., Imai, T., Murayama, S., et al. (2013). The long noncoding RNA nuclear-enriched abundant transcript 1_2 induces paraspeckle formation in the motor neuron during the early phase of amyotrophic lateral sclerosis. Mol. Brain *6*, 31.

Prasanth, K.V., Prasanth, S.G., Xuan, Z., Hearn, S., Freier, S.M., Bennett, C.F., Zhang, M.Q., and Spector, D.L. (2005). Regulating gene expression through RNA nuclear retention. Cell *123*, 249–263.

Raj, A., van den Bogaard, P., Rifkin, S.A., van Oudenaarden, A., and Tyagi, S. (2008). Imaging individual mRNA molecules using multiple singly labeled probes. Nat. Methods *5*, 877–879.

Robinson, M.D., McCarthy, D.J., and Smyth, G.K. (2010). edgeR: a Bioconductor package for differential expression analysis of digital gene expression data. Bioinformatics *26*, 139–140.

Rot, G., Wang, Z., Huppertz, I., Modic, M., Lenče, T., Hallegger, M., Haberman, N., Curk, T., von Mering, C., and Ule, J. (2017). High-Resolution RNA Maps Suggest Common Principles of Splicing and Polyadenylation Regulation by TDP-43. Cell Rep. *19*, 1056–1067.

Rybak, A., Fuchs, H., Smirnova, L., Brandt, C., Pohl, E.E., Nitsch, R., and Wulczyn, F.G. (2008). A feedback loop comprising lin-28 and let-7 controls pre-let-7 maturation during neural stem-cell commitment. Nat. Cell Biol. *10*, 987–993.

Schwenk, B.M., Hartmann, H., Serdaroglu, A., Schludi, M.H., Hornburg, D., Meissner, F., Orozco, D., Colombo, A., Tahirovic, S., Michaelsen, M., et al. (2016). TDP-43 loss of function inhibits endosomal trafficking and alters trophic signaling in neurons. EMBO J. *35*, 2350–2370.

Sephton, C.F., Good, S.K., Atkin, S., Dewey, C.M., Mayer, P., 3rd, Herz, J., and Yu, G. (2010). TDP-43 is a developmentally regulated protein essential for early embryonic development. J. Biol. Chem. *285*, 6826–6834.

Shelkovnikova, T.A., Kukharsky, M.S., An, H., Dimasi, P., Alexeeva, S., Shabir, O., Heath, P.R., and Buchman, V.L. (2018). Protective paraspeckle hyper-assembly downstream of TDP-43 loss of function in amyotrophic lateral sclerosis. Mol. Neurodegener *13*, 30.

Shevtsov, S.P., and Dundr, M. (2011). Nucleation of nuclear bodies by RNA. Nat. Cell Biol. *13*, 167–173.

Standaert, L., Adriaens, C., Radaelli, E., Van Keymeulen, A., Blanpain, C., Hirose, T., Nakagawa, S., and Marine, J.C. (2014). The long noncoding RNA Neat1 is required for mammary gland development and lactation. RNA *20*, 1844–1849.

Tollervey, J.R., Curk, T., Rogelj, B., Briese, M., Cereda, M., Kayikci, M., König, J., Hortobágyi, T., Nishimura, A.L., Zupunski, V., et al. (2011). Characterizing the RNA targets and position-dependent splicing regulation by TDP-43. Nat. Neurosci. *14*, 452–458.

Trapnell, C., Pachter, L., and Salzberg, S.L. (2009). TopHat: discovering splice junctions with RNA-Seq. Bioinformatics *25*, 1105–1111.

Trcek, T., Lionnet, T., Shroff, H., and Lehmann, R. (2017). mRNA quantification using single-molecule FISH in Drosophila embryos. Nat. Protoc. *12*, 1326–1348.

Tsankov, A.M., Akopian, V., Pop, R., Chetty, S., Gifford, C.A., Daheron, L., Tsankova, N.M., and Meissner, A. (2015). A qPCR ScoreCard quantifies the differentiation potential of human pluripotent stem cells. Nat. Biotechnol. *33*, 1182–1192.

Ule, J., Stefani, G., Mele, A., Ruggiu, M., Wang, X., Taneri, B., Gaasterland, T., Blencowe, B.J., and Darnell, R.B. (2006). An RNA map predicting Nova-dependent splicing regulation. Nature *444*, 580–586.

West, J.A., Mito, M., Kurosaka, S., Takumi, T., Tanegashima, C., Chujo, T., Yanaka, K., Kingston, R.E., Hirose, T., Bond, C., et al. (2016). Structural, super-resolution microscopy analysis of paraspeckle nuclear body organization. J. Cell Biol. *214*, 817–830.

Wilusz, J.E., JnBaptiste, C.K., Lu, L.Y., Kuhn, C.D., Joshua-Tor, L., and Sharp, P.A. (2012). A triple helix stabilizes the 3′ ends of long noncoding RNAs that lack poly(A) tails. Genes Dev. *26*, 2392–2407.

Wiśniewski, J.R., Zougman, A., Nagaraj, N., and Mann, M. (2009). Universal sample preparation method for proteome analysis. Nat. Methods *6*, 359–362.

Witten, J.T., and Ule, J. (2011). Understanding splicing regulation through RNA splicing maps. Trends Genet. *27*, 89–97.

Yamazaki, T., Souquere, S., Chujo, T., Kobelke, S., Chong, Y.S., Fox, A.H., Bond, C.S., Nakagawa, S., Pierron, G., and Hirose, T. (2018). Functional Domains of NEAT1 Architectural lncRNA Induce Paraspeckle Assembly through Phase Separation. Mol. Cell *70*, 1038–1053.e7.

STAR★METHODS

KEY RESOURCES TABLE

REAGENT or RESOURCE	SOURCE	IDENTIFIER
Antibodies		
Sox2 monoclonal antibody (D6D9) Alexa 647-conjugated	Cell Signaling	Cat no. 5067; RRID: AB_10828229
Sox2 monoclonal Antibody	Cell Signaling	Cat no. 2748S; RRID: 823640
Nanog monoclonal Antibody	Cell Signaling	Cat no. 8822; RRID: AB_11217637
TDP-43 polyclonal Antibody	Sigma-Aldrich	Cat no. SAB4200006; RRID: AB_10610848
TDP-43 polyclonal Antibody	Proteintech Group	Cat no. 10782-2-AP; RRID: AB_615042
GFP polyclonal Antibody	Molecular Probes/Thermo Fisher	Cat no. A6455; RRID: AB_221570
SFPQ monoclonal Antibody	Thermo Fisher Scientific	Cat no. MA1-25325; RRID: AB_2186931
NONO polyclonal Antibody	Abcam	Cat no. ab70335; RRID: AB_1269576
CPEB1 polyclonal Antibody	Cell Signaling	Cat no. 13583
PSPC1 rabbit polyclonal antibody	Naganuma et al., 2012	
SRSF3 polyclonal antibody	ProteinTech Group	Cat no. 10916-1-AP; RRID: AB_2185064
TNPO1 monoclonal antibody	Abcam	Cat no. ab10303; RRID: AB_2206878
U2AF2 monoclonal antibody	Sigma-Aldrich	Cat no. U4758; RRID: AB_262122
Brachyury N-19 goat polyclonal antibody	Santa Cruz Biotechnologies	Cat no. sc17743; RRID: AB_634980
Foxa2 (HNF-3β) M-20 goat polyclonal	Santa Cruz Biotechnologies	Cat no. sc-6554; RRID: AB_2262810
RFP rabbit polyclonal	Rockland	Cat no. 600-401-379S; RRID: AB_2209751
Donkey anti-rabbit IgG 555	Invitrogen	Cat no. A31572; RRID: AB_162543
Donkey anti-goat IgG 488	Invitrogen	Cat no. A11055; RRID: AB_2534102
Histone H3 polyclonal Antibody	Abcam	Cat no. ab1791; RRID: AB_302613
Beta Actin polyclonal Antibody	New England Biolabs/Cell Signaling antibody	Cat no. 8H10D10; RRID: AB_2242334
RNAPolII-S5,S2	Abcam	Cat no. ab103968; RRID: AB_2687918
DyLight 650-conjugated anti SSEA-1 (clone MC-480)	Thermo Fisher	Cat no. MA1-022-D650; RRID: AB_2536696
Alexa Fluor 647-conjugated anti TRA-1-60	BD Bioscience	Cat no. 560122; RRID: AB_1645448
Alexa Fluor 647 Dk anti-Gt IgG (H+L)	Thermo Fisher	Cat no. A11058; RRID: AB_2534105
Goat anti-rabbit IgM-HRP	Santa Cruz Biotechnology	Cat no. sc-2030; RRID: AB_631747
Goat anti-mouse IgG HRP-conjugated	Dianova	Cat no. 115-035-003; RRID: AB_10015289
Chemicals, Peptides, and Recombinant Proteins		
(Z)-4-Hydroxytamoxifen	Sigma-Aldrich	H7904
Neurobasal Medium	Thermo Fisher	21103049
DMEM F12	Thermo Fisher	11320033
N2	Thermo Fisher	17502048
B27	Thermo Fisher	17504044
Glutamax	Thermo Fisher	35050
1% nonessential amino acids	Thermo Fisher	1140050
2-mercaptoethanol	Thermo Fisher	31350-010
MEK inhibitor PD0325901	Axon Medchem	1408
GSK3 inhibitor CHIR99021	Tocris	4953/50
LIF	produced in house	SV30160.03HI
Trypsin-EDTA	Thermo Fisher	25200056
HyClone Fetal Bovine Serum (FBS)	GE Healthcare	SV30160.03HI
mTeSR1 medium	Stem Cell Technologies	058-50

(*Continued on next page*)

Continued

REAGENT or RESOURCE	SOURCE	IDENTIFIER
Matrigel	Cornig	356234
Gentle Cell Dissociation Reagent	StemCell Technologies	7174
KnockOut Serum Replacement	Thermo Fisher	10828028
DMEM high glucose	Thermo Fisher	11965092
Blue Sepharose 6 Fast Flow/ HisTrap HP columns	GE LifeSciences	17-0412-01
recombinant WNT3A	D. Ten Berge	N/A
Retinoic Acid	R2625-50MG	Sigma
recombinant BMP4	R&D systems	314-BP
Accutase	Sigma-Aldrich	A6964
Y-27632 ROCK inhibitor	R&D systems	1254/10
RPMI1640	Thermo Fisher	11875093
L-Glutamine	Thermo Fisher	25030081
B27 supplement without insulin	Thermo Fisher	A1895601
Lipofectamine 3000	Thermo Fisher	L3000008
Lipofectamine RNAiMAX	Thermo Fisher	13778150
Puromycin	Sigma-Aldrich	P8833-10MG,
blasticidine	Invivogen	ant-bl-05
G418	Invivogen	ant-gn-01
Trizol LS	Life Technologies	10296028
QIAzol	QIAGEN	79306
Zymo Direct-zol	Zymogen	R2052
RNeasy Mini Kit	QIAGEN	74104
SuperScript III Reverse Transcriptase	Thermo Fisher	18080085
RNase H, recombinant	New England Biolabs	M0297S
miRNeasy Micro Kit	QIAGEN	217084
KOD FX Neo enzyme	Toyobo	KFX-201
Taqman assay master mixl	Thermo Fisher	4369514
Q5® High-Fidelity 2X Master Mix	Thermo Fisher	M0492
miScript PCR Starter Kit	QIAGEN	218193
formamide	Calbiochem	4610-OP
Dextran Sulfate	VWR	9011-18-1
competitor tRNA from E.coli	Roche Diagnostics	10109541001
methanol-free formaldehyde	Thermo Fisher	28906
digoxigenin (DIG) RNA labeling kit	Roche	11175025910
2-well μ-Slides	Ibidi	80286
8-chambr Slides	Ibidi	80826
DAPI	New England Biolabs	9071S
SYTOX Blue Dead Cell Stain, for flow cytometry	Thermo Fisher	S34857
UltraPure BSA	Thermo Fisher	AM2616
vanadyl-ribonucleoside complex	New England Biolabs	S1402S
Insulin (human recombinant - yeast)	Life Tech	12585-014
Transferrin (human recombinant)	Sigma-Aldrich	T3705-1G
Sodium selenite	Sigma-Aldrich	S5261-10G
Ascorbic acid 2-phosphate	Sigma-Aldrich	A8960-5G
FGF2 (human recombinant - *E. coli*)	Peprotech	100-18B (1 mg)
TGFB (human recombinant - *E. coli*)	Peprotech	100-21 (100 ug)
TURBO Dnase	Thermo Fisher	am2238
RNeasy MinElute RNA cleanup	QIAGEN	74204

(*Continued on next page*)

Continued

REAGENT or RESOURCE	SOURCE	IDENTIFIER
protease inhibitors	Merck Millipore	539134
phosphatase inhibitors	Sigma-Aldrich	4906837001
proteasome inhibitor	Sigma -Aldrich	MG132
Mini-PROTEAN TGX Stain Free Gels, 4-15%	Bio-Rad Laboratories	456-8086
Clarity Western ECL Substrate	Bio-Rad Laboratories	170-5060
5% milk powder	Carl Roth	T145.1
RNasin Plus RNase inhibitor	Promega	PRN2615
Lys-C	Wako Chemicals	125-02543
Trypsin	Promega	V5111
Igepal CA-630	Sigma-Aldrich	I8896
Triton X-100	Sigma-Aldrich	9002-93-1
Protein A Dynabeads	Thermo Fisher	10002D
RNase I	Ambion	AM2295
RNase A	Nacalai Tesque	9001-99-4
Proteus Clarification Mini Spin Column	Generon	GEN-MSF500
ssRNA ligase	New England Biolabs	M0204S
PEG400	Sigma-Aldrich	202398
sodium butyrate	Sigma-Aldrich	B5887-250MG
ascorbic acid	Sigma-Aldrich	A8960
Hydrocortisone	Sigma-Aldrich	H0396
Insulin	Thermo Fisher	12585014
Protan BA85 Nitrocellulose Membrane	Thermo Fisher	LC2009
proteinase K	Roche	3115828001
Phase Lock Gel Heavy tube	713-2536	VWR
Glycoblue coprecipitant	Ambion	9516
Costar SpinX column	Corning Incorporated	8161
CircLigase ssDNA	Epicenter	CL4111K
Accuprime Supermix 1	Thermo Fisher	Accuprime Supermix 1
Agencourt AMPure XP beads	Beckman-Coulter	Agencourt AMPure XP beads
Critical Commercial Assays		
P3 Primary Cell 4D-Nucleofector Kit	Lonza	V4XP-3012
Nucleofector Kit V	Lonza	VCA-1003
RiboZero	Epicenter	Cat# MRZG12324
TruSeq stranded total RNA Sample Prep Kit	Illumina	Cat# 20020599
QuantSeq mRNA 3′ end sequencing kit	Lexogen	Cat# SKU 015.96 and SKU 016.96
alkaline phosphatase staining	Sigma-Aldrich	AB0300-1KT
Agilent 2100 Bioanalyzer with RNA Pico 6000 kit	Agilent	5067-1513
Qubit dsDNA HS Assay Kit	Thermo Fisher	Q32854
Inside Stain kit	Miltenyi Biotech	130-090-477
Nucleofector MEF 1 Kit	Lonza	VPD-1004
Nascent RNA Capture Kit	Thermo Fisher	C10365
Deposited Data		
QuantSeq and RNaseq libraries to study developmental alternative polyadenylation in hESC, its progeny and upon TDP-43 KD	This paper	E-MTAB-5090. Accessible via https://www.ebi.ac.uk/arrayexpress/
RNaseq libraries to study developmental alternative polyadenylation in human primitive streak progenitors derived from hESCs.	This paper	E-MTAB-5099. Accessible via https://www.ebi.ac.uk/arrayexpress/

(*Continued on next page*)

Continued

REAGENT or RESOURCE	SOURCE	IDENTIFIER
QuantSeq libraries to study TDP-43 dependent alternative polyadenylation in mESCs and upon paraspeckles/TDP43 perturbations	This paper	E-MTAB-5091. Accessible via https://www.ebi.ac.uk/arrayexpress/
RNaseq libraries to study TDP-43 dependent alternative polyadenylation in mESCa and cTdp43KO	This paper	E-MTAB-5097. Accessible via https://www.ebi.ac.uk/arrayexpress/
iCLIP datasets for TDP-43	This paper	E-MTAB-5100. Accessible via https://www.ebi.ac.uk/arrayexpress/
Nascent RNaseq in conjunction with Illumina TRUseq method to sequence total RNAs including short lived RNAs using highly strand-specific next-generation sequencing (NGS) libraries	This paper	E-MTAB-5115
QuantSeq libraries to study gene expression changes in Neat1ΔpA compared to parental undifferentiated hESCs	This paper	Accessible via https://expressrna.org/
Fractionation RNaseq in conjunction with Illumina TRUseq method	This paper	E-MTAB-5116
RNaseq differentiation of hESCs to endoderm, mesoderm, ectoderm, and hepatoblasts	Gifford et al., 2013	GSM1112847, GSM1112845, GSM1112846, GSM1112844, GSM1112835, GSM1112833, GSM1112834, GSM1112837, GSM1124072, GSM1124072
iCLIP datasets for TDP-43 in SH-SY5Y cells	Tollervey et al., 2011	E-MTAB-527 Accessible via https://www.ebi.ac.uk/arrayexpress/
Analysis of Pro-Inflammatory Gene Activation and RNA Processing by RNaseq of Nascent Transcripts I		GSE32916 and GSE38892, accessible via GEO accession viewer
Mendeley dataset; Additional data composed of Sanger sequencing and confirmatory gel electrophoresis confirming the CRISPR-Cas9 edited human and mouse embryonic stem cells.	This paper and Mendeley data	https://data.mendeley.com/datasets/hbr8p7n526/2
Experimental Models: Cell Lines		
HEK293 Flag-WT TDP-43 tetracycline inducible	Budini et al., 2015	
HeLa	ATCC: CCL-2	RRID: CVCL_0045
primary neonatal human dermal fibroblast (NHDF)	ATCC	CRL-2522
secondary human fiboblasts (HiF-Ts)	Cacchiarelli et al., 2015	
HAP1	ATCC	204508
hESCs H9	Wicell	WB66593
V6.5 mESCs	ATCC	SCRC-2011
e14tg2a ICE	ATCC	SCRC-1029
cTdp-43 KO	Ling et al., 2015	
IDG3.2	Hitz et al., 2007 (C57BL/6J x 129S6/SvEvTac)F1 mESC line	
Experimental Models: Organisms/Strains		
Mouse: CD-1	Charles River	Mouse: CD-1
Mouse: mT/mG	Muzumdar et al., 2007	Mouse: mT/mG
Oligonucleotides		
Stellaris smFISH Probe: Human NEAT1 Middle Segment with Quasar 570	Stellaris	SMF-2037-1-BS
Stellaris smFISH Probe: Human NEAT1 5‘ segment conjugated to Quasar®670 or Quasar®570	Stellaris	SMF-2036-1
Stellaris smFISH Probe: Mouse Neat1 middle segment conjugated to Quasar®670	Stellaris	Customized product
Stellaris smFISH Probe: Mouse Neat1 5‘ segment conjugated to Quasar®570	Stellaris	Customized product

(*Continued on next page*)

Continued

REAGENT or RESOURCE	SOURCE	IDENTIFIER
Stealth RNAi siRNA	Thermo Fisher Scientific	12935-200
TDP-43 siRNA, 5′-GGCUCAAGCAUGGAUUCUA-	Dharmacon	Customized product
GAPDH_F		GCTCATTTCCTGGTATGACAACG
GAPDH_R		GAGATTCAGTGTGGTGGGGG
OCT4_F		CAATTTGCCAAGCTCCTGAAG
OCT4_R		AAAGCGGCAGATGGTCGTT
MESP_F		CTGCCTGAGGAGCCCAAGT
MESP_R		GCAGTCTGCCAAGGAACCA
T_F		CAACCTCACTGACGGTGAAAAA
T_R		ACAAATTCTGGTGTGCCAAAGTT
MIXL_F		CCGAGTCCAGGATCCAGGTA
MIXL_R		CTCTGACGCCGAGACTTGG
SOX17_F		GGCGCAGCAGAATCCAGA
SOX17_R		CCACGACTTGCCCAGCAT
Lefty1_F		TGTACATTGACCTGCAGGG
Lefty1_R		ACTCATAAGCCAGGAAGCC
EOMES_F		ACAGGAGATTTCATTCGGG
EOMES_R		TTGTAAGACTATCATCTGGGTG
GDF3_F		GAGACTTATGCTACGTAAAGGA
GDF3_R		GGTAAAGAAAGAAACCTTGGTC
FOXD3_F		CTACTACAGGGAGAAGTTCCC
FOXD3_R		GTTGAGTGAGAGGTTGTGG
Neat1.screen_F		GTTTGGCTTGAATGGTGCTT
Neat1.screen_R		CTTCCCTCCCAGAGAGTTGA
NEAT1pA.screen_F		TGAGCCAAGACTAGAGGGGA
NEAT1pA.screen_R		CCTTGCTGCTCCCTTTGAAA
Neat1.screen_F		GTTTGGCTTGAATGGTGCTT
Neat1.screen_R		CTTCCCTCCCAGAGAGTTGA
Sox2Δmir21.screen_F		TTAACGCAAAAACCGTGATG
Sox2Δmir21.screen_R		GGCAGCCTGATTCCAATAAC
Neat1ΔTH.screen_F		TTACTGCACCAGACCCTGTC
Neat1ΔTH.screen_R		TCCTTTGGGGAACAGGAAAGAG
Gapdh_F		TTCACCACCATGGAGAAGGC
Gapdh_R		CCCTTTTGGCTCCACCCT
Neat1_1_F		TTGGGACAGTGGACGTGTGG
Neat1_1_R		TCAAGTGCCAGCAGACAGCA
Neat1_2_F		GATCGGGACCCCAGTGACCT
Neat1_2_R		AGCTTTCCCCAACACCCACA
mmu-mir-21	QIAGEN	MIMAT0000076: 5′UAG CUU AUC AGA CUG AUG UUG A, MIMAT0004494: 5′CAA CAC CAG UCG AUG GGC UGU
TaqMan Gene Expression Assay NEAT1, isoform v2	Thermo Fisher	Hs03924655_s1
TaqMan Gene Expression Assay, Gene Symbol: SOX2	Thermo Fisher	Hs01053049_s1
TaqMan Gene Expression Assay, Gene Symbol: GAPDH	Thermo Fisher	Hs02758991_g1
TaqMan Gene Expression Assay, Neat1, Gene Symbol NEAT1 isoform v1	Thermo Fisher	Hs01008264_s1
TaqMan Gene Expression Assay, Gene Symbol POU5F1	Thermo Fisher	Hs00999632_g1

(*Continued on next page*)

Continued

REAGENT or RESOURCE	SOURCE	IDENTIFIER
TaqMan® Gene Expression Assay, Gene Symbol SCARNA10	Thermo Fisher	Hs03309805_s1
TaqMan® Gene Expression Assays, gene symbol Neat1v1	Thermo Fisher	Mm03455878_s1
Recombinant DNA		
pmaxGFP plasmid with insertions of modified SOX2-UTR	Addgene	16007
PMIRH21PA-1-GVO-SBI	System Biosciences	PMIRH21PA-1-GVO-SBI
PX330-B/B	Addgene	42230
pcDNA6/TR	Addgene	5676
pCXLE-hMLN	Addgene	27079
MIP 247 CoMiP 4in1 with shRNA p53.	Addgene	63726
Software and Algorithms		
Bowtie2		http://bowtie-bio.sourceforge.net/bowtie2/index.shtml
TopHat2		RRID: SCR_013035; http://tophat.cbcb.umd.edu/
STAR	Dobin et al., 2013	RRID: SCR_015899; https://github.com/alexdobin/STAR
Cufflinks		RRID: SCR_014597; http://cole-trapnell-lab.github.io/cufflinks
expressRNA	Rot et al., 2017	http://www.expressrna.org/
BLAST+/2.3.0		RRID: SCR_001598; https://blast.ncbi.nlm.nih.gov/Blast.cgi
R	R Project for Statistical Computing	RRID: SCR_001905; http://www.r-project.org/
DEXseq		https://github.com/roryk/DEXSeq/
Progenesis QI software	version 2.0, Nonlinear Dynamics	
Mascot (version 2.5.1)	Matrix Science	http://www.matrixscience.com/whats_new/mascot-2-5-1-patch-release.html
EdgeR	Robinson et al., 2010	https://bioconductor.org/packages/release/bioc/html/edgeR.html
iCount		http://icount.fri.uni-lj.si/
HTSeq		https://htseq.readthedocs.io/en/release_0.11.1/
Other		
NEATΔpA.gRNA.up.fwd		CACCGATGCAAACAATTACTGTCGT
NEATΔpA.gRNA.up.rev		AAACACGACAGTAATTGTTTGCATC
NEATΔpA.gRNA.down.fwd		CACCGTGTTGAGAGTTGGTAATCAT
NEATΔpA.gRNA.down.rev		AAACATGATTACCAACTCTCAACAC
Neat1ΔpA.gRNA.up.fwd		caccGAAGCTTCTTAGAATTGTCA
Neat1ΔpA.gRNA.up.rev		aaacTGACAATTCTAAGAAGCTTC
Neat1ΔpA.gRNA.down.fwd		caccGAGGGGAGGAAAATGGTTAGT
Neat1ΔpA.gRNA.down.rev		aaacACTAACCATTTTCCTCCCCTC
Neat1ΔTDP43.gRNA.up.fwd		caccgTTGTGAAAACCCTGTATATG
Neat1ΔTDP43.gRNA.up.rev		aaacCATATACAGGGTTTTCACAAc
Neat1ΔTDP43.gRNA.down.fwd		caccGTGAAGAAAGCTGTAACTGC
Neat1ΔTDP43.gRNA.down.rev		aaacGCAGTTACAGCTTTCTTCAC
Sox2Δmir21_gRNA1_up		caccgAGTATTTATCGAGATAAACA
Sox2Δmir21_gRNA1_down		aaacTGTTTATCTCGATAAATACTc

(*Continued on next page*)

Continued

REAGENT or RESOURCE	SOURCE	IDENTIFIER
Sox2Δmir21_gRNA2_up		caccgATTTAGGACCGTTACAAACA
Sox2Δmir21_gRNA2_down		aaacTGTTTGTAACGGTCCTAAATc
Neat1ΔTH_gRNA1_fwd		caccgaaggaagcacggtactgca
Neat1ΔTH_gRNA1_rev		AAACtgcagtaccgtgcttccttc
Neat1ΔTH_gRNA2_fwd		caccgAGGAAAAGAAACACCTGCGG
Neat1ΔTH_gRNA2_rev		aaacCCGCAGGTGTTTCTTTTCCTc

CONTACT FOR REAGENT AND RESOURCE SHARING

Further information and requests for resources and reagents should be directed to and will be fulfilled by Micha Drukker (micha.drukker@helmholtz-muenchen.de).

EXPERIMENTAL MODEL AND SUBJECT DETAILS

Cell culture

All mouse ESC lines e.g., e14tg2a, IDG3.2 (Hitz et al., 2007) and tamoxifen inducible (concentration of 1ug/mL or ~2.5uM of (Z)-4-Hydroxytamoxifen, H7904, Sigma-Aldrich) *Tardbp* conditional knockout (termed cTdp-43 KO (Ling et al., 2015)) were maintained on 0.1% gelatin-coated plates in 1:1 Neurobasal (21103049) DMEM (11320033) medium containing N2 (17502048) and B27 (17504044) supplements, 1% Glutamax (35050), 1% nonessential amino acids (1140050), 0.1 mM 2-mercaptoethanol (31350-010) (all Thermo Fisher Scientific), 1 μM MEK inhibitor PD0325901 (1408, Axon Medchem), 3 μM GSK3 inhibitor CHIR99021 (4953/50 Tocris), and 1,000 U/ml LIF (produced in-house), a condition named 2iLIF. Cells were passaged using 0.25% Trypsin-EDTA (25200056, Thermo Fisher Scientific). Spontaneous differentiation was induced by the removing pathway inhibitors and LIF and replacing N2B27 supplements with 10% HyClone Fetal Bovine Serum (FBS) (SV30160.03HI GE Healthcare). Fresh medium was applied daily.

HESCs (line H9) were maintained in mTeSR1 medium (05850, STEMCELL Technologies) on Matrigel-coated plates (356234, Corning) prepared by 1:100 dilution, and 5 mL coating of 10 cm plates for 1 h at 37°C. Colonies were passaged using the gentle cell dissociation reagent (07174, StemCell Technologies). HESCs were differentiated by Trypsin-EDTA, dissociation to single cells and seeding (100,000 cells/cm2) on Matrigel-coated plates in DMEM/F12 medium (11320), supplemented with 20% KnockOut Serum Replacement (KSR; 10828028, Thermo Fisher Scientific), Glutamax, nonessential amino acids, and β-mercaptoethanol, or B27 supplemented as above with either 10 μM CHIR99021, 250ng/ml recombinant WNT3A (kindly provided by Derk ten Berge), 0.5 μM RA (R2625, Sigma-Aldrich) or 50ng/ml BMP4 (314-BP; R&D Systems). Fresh medium was applied daily.

HEK293T Flag-WT TDP-43 tetracycline inducible cell line was cultured as previously described (Budini et al., 2015). These HEK cells were transfected using Lipofectamine 3000 (L3000001, Thermo Fisher Scientific) according to manufacturer's instructions. Fresh medium was applied daily. All cells were grown at 37oC in 5% CO2.

Generation of h/mESC lines harboring edited NEAT1/Neat1

The *NEAT1ΔpA* hESC line was generated by deleting a 500 nt region surrounding the proximal pA site including the regulatory *cis*-elements (Naganuma et al., 2012). Based on Raj et al. (2008) forward and reverse gRNAs (listed below) with *BbsI* restriction site overhangs were designed, phosphorylated, annealed and cloned into *BbsI* digested Cas9-2A-GFP vector (48138 Addgene). One million cells were transfected with 5 μg plasmid pairs using the P3 Primary Cell 4D-Nucleofector Kit (V4XP-3012 Lonza) and the 4D-Nucleofector Platform (Lonza), program CB-156. 10-14 days later clones were picked, expanded and PCR-screened for identifying clones with alleles harboring deletions.

A similar approach was used for deleting 60 nt surrounding the proximal pA site in *Neat1*, 100 nt corresponding to the UGUG-rich TDP-43 binding site in *Neat1*, the region corresponding to the triple helix (*ΔTH*) in *Neat1_2*, and *miR-21* binding site in *Sox2*. 5×10^5 mESCs were plated on 0.2% gelatin-coated wells of a 6 well plate, and were transfected 3 h later (Lipofectamine 3000, L3000008, Thermo Fisher Scientific) with 2 μg total plasmid DNA made of a pair of SpCas9-2A-Puro plasmids (Plasmid #62988, Addgene), each containing single guide RNAs targeting the respective forward or reverse region in *Neat1* (listed below). 48 h later the cells were reseeded and treated with media supplemented with 1 μg/ml puromycin (P8833, Sigma-Aldrich). 5-6 days later clones were picked, expanded in 96-well plates and PCR-screened for identifying clones with alleles harboring deletions. Sequences of gRNAs and primers used for generating and screening genetically edited h/mESCs are listed in the STAR Methods section

Generation of HAP-1 cells harboring edited NEAT1

PX330-B/B containing two sgRNAs (2 ug) and pcDNA6/TR (0.2 ug) containing the blasticidin resistance gene (Thermo Fisher Scientific) were co-transfected into HAP1 cells (1.5×10^6 cells) by Nucleofector Kit V (VCA-1003, Lonza) with a Nucleofector device (Lonza)

using program "X-005" according to the manufacturer's instructions. To enrich the plasmid-transfected cells, the HAP1 cells were treated with 20 ug/ml blasticidin (ant-bl-05, InvivoGen) for 3 days, starting 1 day after transfection. Subsequently, the cells were diluted into 96-well plates for creating clones. Clones were lysed by proteinase K (200 ug/ml, 3115828001 Roche, 20 mM Tris-HCl pH 8.0, 5 mM EDTA, 400 mM NaCl, and 0.3% SDS at 55°C for 1 h, followed by proteinase K inactivation (95°C for 15 min). Then, the lysates were subjected to PCR analysis to amplify the genomic regions flanking the guide RNA target sites for detecting deletions or insertions using KOD FX Neo enzyme (KFX-201, TOYOBO). The indel-positive clones were further confirmed by sequencing.

Specifically, to establish HAP1 *NEAT1 ΔUG* cell line lacking three *NEAT1_2* domains (5942-7025 nt, 9201-11091 nt, and 21061-22012 nt), these domains were deleted by sequential CRISPR/Cas9-mediated deletions. First, *NEAT1_2* 5942-7025 nt (5.9-7 kb) domain was deleted by sgRNAs (GGCGGGTCGTCCTAACTAGC and CATTTAAACCTTCTTCCCCG) in HAP1 WT cells. Second, *NEAT1_2* 21061-22012 nt (21-22 kb) was deleted by introducing two sgRNAs (TACGCGGGGAAACGTGCCAC and TCCGACTT CATTTCGAGTGA) into HAP1 Δ5.9-7 kb cells. Third, *NEAT1_2* 9201-11091 nt was deleted by introducing two sgRNAs (GTACCTTA TAACGTTGGATT and TATTACCTTGGCCTAGGGGG) into HAP1 Δ5.9-7 kb/21-22 kb cells to establish *NEAT1 ΔUG* cell lines. To establish HAP1 *NEAT1 ΔUG/UGx60* cell line by knocking-in UG repeats (UG x 60) into the HAP1 *NEAT1 ΔUG* cell line, PX330-B/B (2 ug) containing two sgRNAs targeting to knock-in vector (GCATCGTACGCGTACGTGTT) and NEAT1 genomic region (*NEAT1_2* 22.1 kb region) (GCGGGCGTCTGCGTGACCTC) were co-transfected with knock-in vector (pcDNA3) containing 60 TG repeats (generated by Genscript) and pcDNA6/TR plasmids (0.2 ug) into HAP1 *NEAT1 ΔUG* cells as described above. The insertion was detected by PCR and further confirmed by sequencing.

Overexpression of TDP-43

A mESC line (parental e14tg2a, kindly provided by Michael Kyba) harboring doxycycline inducible i*TDP-43-eGFP* transgene was generated by targeting the *Rosa26* locus of the A2lox.Cre line with the p2lox (plasmid #34635, Addgene) construct cloned with TDP-43-eGFP fusion cassette. The recombination was performed as previously described (Kyba et al., 2002), and 24 h after transfection cells were selected with 250 ng/ml G418 (Invivogen, ant-gn-1) for 7 days. Clones were picked, expanded and validated. This line was subsequently modified by deleting the 100 nt corresponding to the UGUG-rich TDP-43 binding site in *Neat1*. Constitutive overexpression of TDP-43 during human fibroblast reprogramming was mediated by transduction or transfection of myc-tagged *TDP-43* (Schwenk et al., 2016). Empty vector was used as a control.

Knockdown of TDP-43

2x10^5 Accutase-treated single hESCs were seeded 24 h prior to transfection on Matrigel-coated 6-well plates with mTeSR1 medium supplemented with ROCK inhibitor. Per well, siRNA transfection was performed using 5 μM siRNA duplexes mixed with 5 μL Lipofectamine RNAiMAX (13778150, Thermo Fisher Scientific) and 100 μL DMEM, a solution incubated at RT for 20 min. Dharmacon, A-012394-14, TARDBP: 5′-GGCUCAAGCAUGGAUUCUA-3′ was used to target TDP-43, and a Stealth RNAi siRNA (12935-200, Thermo Fisher Scientific) was used as the negative control. Transduction was used for knocking-down of *TDP-43* via shRNAs for global analysis of PASs in parallel to the use of a luciferase shRNA vector as a control (Schwenk et al., 2016).

Plasmids

The 3′ UTR of *SOX2* was ectopically express by cloning the complete UTR (1263 nt including 100 nt downstream of distal pA site) immediately after the coding sequence of *eGFP* in the pmaxGFP plasmid (#16007 addgene), producing the pmaxGFP-SOX2-UTR construct. Two variants of this plasmid were prepared by deleting the *miR-21* binding site (AAATGTCCATTGTTTATAAGCTGA) producing pmaxGFP-SOX2-UTRΔmiR21, or the regulatory sequence spanning the proximal pA site (GGAAATGGGAGGGGTGCAAAA GAGGAGAGTAAGAAACGCATGGAGAAAACCCGGTACGCTCAAAAAGAAAAAGGAAAAAAAAAAATCCCATCA) producing pmaxGFP-SOX2UTRΔpA. To ectopically express *miR-21*, the GFP sequence of plasmid PMIRH21PA-1-GVO-SBI (System Biosciences), which codes for the microRNA precursor of *miR-21*, was replaced by the sequence of the gene encoding tdTomato fluorescent protein.

Reprogramming of human fibroblasts

1.5x10^6 primary neonatal human dermal fibroblast (NHDF) (ATCC, CRL-2522) were transfected using the Nucleofector MEF 1 Kit (VPD-1004, Lonza) with 6μg of plasmid MIP 247 CoMiP 4in1 and 3ug of pCXLE-hMLN (63726 and 27079, Addgene). Cells were pulsed with T-020 or N-024 program using Nucleofector 2b (AAB-1001, Lonza), and were plated on Matrigel-coated plates with fibroblast medium composed of DMEM high glucose (11965092, Thermo Fisher Scientific), 10% HyClone Fetal Bovine Serum (SV30160.03HI GE Healthcare), 0.1mM sodium butyrate (B5887-250MG, Sigma Aldrich) and 64 μg/mL ascorbic acid (A8960, Sigma Aldrich). On day 2, media was changed to Essential 7 media: DMEM/F12, (11320033), Insulin (12585014) both Thermo Fisher Scientific, human recombinant Transferrin (T3705), Sodium selenite (S5261), Ascorbic acid 2-phosphate (A8960) by Sigma Aldrich and FGF2, (100-18B, Peprotech), supplemented with 0.1 mM sodium butyrate, 0.1mM Hydrocortisone (H0396, Sigma Aldrich) and 64 μg/mL ascorbic acid. Between days 10-15 first iPSC-like colonies appeared, after medium was changed to Essential 8 medium (E7 + 2ng/ml TGFbeta1) (100-21, Peprotech)) supplemented 64 μg/mL ascorbic acid in low O_2 (5% O2) conditions. For

reprogramming of secondary human fibroblasts (HiF-Ts), cells were cultured and reprogrammed as described (Cacchiarelli et al., 2015). The number of reprogrammed colonies was analyzed by alkaline phosphatase staining (AB0300-1KT, Sigma Aldrich).

ANIMALS

Generation of chimeras

Tetraploid chimeras were generated according to standard protocols (Engert et al., 2013). Embryos were collected from the mT/mG expressing mouse line (Muzumdar et al., 2007), maintained on C57/Bl6J background.

Animal data

Mouse keeping was done at the central facilities at HMGU in accordance with the German animal welfare legislation and acknowledged guidelines of the Society of Laboratory Animals (GV-SOLAS) and of the Federation of Laboratory Animal Science Associations (FELASA).

Immunofluorescence of embryos

Immunofluorescence whole-mount staining was performed in the following way. Briefly, embryos were isolated, fixed for 20 minutes using 2% PFA in PBS, permeabilized using 0.1% Triton X-100 in 0.1 M glycine pH 8.0. After blocking using 10% FCS, 3% donkey serum, 0.1% BSA, 0.1% Tween 20 for 2 h, embryos were incubated with the primary antibody o/n at 4°C in blocking solution. After several washes in PBS containing 0.1% Tween-20 (PBST) embryos were incubated with secondary antibodies (donkey anti-goat 488, donkey anti-rabbit 555 each 1:800) in blocking solution for 3 h. During the final washes with PBST, embryos were stained with 4′,6-diamidino-2-phenylindole, dihydrochloride (DAPI), transferred into 15% and 30% glycerol and embedded between two coverslips using 120μ m Secure-Seal spacers (Invitrogen, S24737) and ProLong Gold antifade reagent (Invitrogen, P36930). Antibodies: Foxa2 1:1000 (Santa Cruz, sc-6554), Brachyury 1:500 (N-19, Santa Cruz, sc17743), RFP 1:1000 (Rockland, 600-401-379S).

METHOD DETAILS

RNA preparation and qRT-PCR assays

Total RNA was prepared from cell pellets using miRNeasy Micro Kit (217084, QIAGEN) according to the manufacturer's instructions. First-strand cDNA synthesis of 1 μg total RNA was performed using SuperScript III Reverse Transcriptase (18080085, Invitrogen), according to the manufacturer's guidelines. qRT-PCR reactions were performed using Power SYBR Green Master Mix (4367659, Thermo Fisher Scientific). *miR-21* was analyzed using the miScript protocol (218193, QIAGEN). Primers used in this study are listed in the STAR Methods section

RNA sequencing

3 μg total RNA was treated with TURBO DNase (am2238, Thermo Fisher Scientific) according to manufacturer's instructions followed by RNeasy MinElute RNA cleanup (74204, QIAGEN). Microcapillary electrophoresis on Agilent 2100 Bioanalyzer with RNA Pico 6000 kit (5067-1513, Agilent) was used to analyze RNA quality (RIN values > 8). For total RNA sequencing and per library, 1 μg RNA was depleted of rRNA using RiboZero Gold (Human/Mouse/Rat) kit followed by a cleanup step and library preparation using TruSeq Stranded Total RNA kit (RS-122-2301, Illumina) and 11 cycles of PCR, followed by purification with Agencourt AMPure XP beads (Beckman-Coulter, A63881). Libraries were evaluated on an Agilent 2100 Bioanalyzer using the DNA 1000 kit (5067-1504, Agilent) and DNA concentration was measured using a Qubit dsDNA HS Assay Kit (Q32854 Thermo Fisher Scientific). Samples were sequenced using HiSeq2500 to generate 50-nt single-end reads, sequencing depth was 20–40 Mio reads per library. For 3′mRNaseq, 0.5 μg DNase-treated RNA was used per library prepared using Lexogen QuantSeq-REV kit (016, Lexogen GmbH) according to manufacturer's instructions, and using poly(T) primer for reverse transcription. The library was sequenced using Illumina HiSeq, producing 60 nt single-end reads.

For nascent RNA-Seq, metabolic RNA labeling in living undifferentiated hESCs was performed by adding 0.4mM EU (5-ethynyl uridine) to the medium for 40 min. Total RNA was prepared using RNeasy MinElute RNA cleanup, and 10 μg of total RNA was treated by Ribo-Zero Gold rRNA removal kit, and purified using RNeasy MinElute cleanup kit. rRNA-depleted, EU-labeled RNA (0.5-1 μg) was biotinylated and captured using Click-it Nascent RNA Capture Kit (C10365, Thermo Fisher Scientific) according to manufacturer's instructions. Libraries were prepared using TruSeq Stranded Total RNA kit and sequenced on Illumina NexSeq 500 instrument with 75 cycles of single-end reads.

Western blotting

Cells were trypsinized and lysed using RIPA buffer, containing phosphatase (Sigma-Aldrich, 4906837001) and protease (Merck, 539134) inhibitors. After addition of 2x SDS loading buffer with 2-Mercaptoethanol (Sigma-Aldrich, M3148) samples were heated to 95°C for 5 min. Samples were ran on Mini-PROTEAN TGX Stain Free Gels, 4%–15% (Bio-Rad Laboratories, 456-8086), and blotted using the Mini Trans-Blot Cell (Bio-Rad Laboratories, 1703930). Following 3 × 5 min washes with TBS-T, membranes were blocked with 5% milk powder (T145.1, Carl Roth) in TBS-T. Membranes were then incubated o/n at 4°C with 5% milk powder in TBS-T containing the primary antibody. After 3 × 5 min TBS-T washes, membrane was incubated with goat anti-rabbit IgM-HRP (sc-2030, Santa Cruz) or Goat anti-mouse IgG HRP-conjugated (115-035-003 Dianova) in 5% milk powder in TBS-T. Following 4 15 min washes

with TBS-T the membrane was incubated for 1 min with Clarity Western ECL Substrate (170-5060, Bio-Rad Laboratories) and imaged with ChemiDoc MP System (Bio-Rad Laboratories) or exposed to X-ray film. Antibodies used are listed in the STAR Methods.

Immunofluorescence

Cells were grown in Matrigel coated 8 well chamber slides (80826, Ibidi) and fixed with 4% PFA/DPBS solution (Thermo Fisher Scientific 16% Formaldehyde (w/v), Methanol-free, 28906) for 15 min at RT and permeabilized using 0.2% Triton X-100/DPBS solution for 15 min at RT. Primary and secondary antibodies were diluted per manufacturer recommended concentrations in 10%FBS/0.2% Triton X-100/DPBS and incubated respectively o/n at 4°C and 1 h at RT. The samples were washed with DAPI (50ug/ml) solution and imaged using a Zeiss Axiovert 200M epifluorescent microscope. Antibodies used are listed in the STAR Methods.

Flow cytometry

Plates were washed with PBS, and cells were dissociated by Trypsin-EDTA, followed by resuspension in 2% FBS 1mM EDTA PBS buffer, and incubation with antibodies for 30-60 min on ice. Cells were centrifuged, resuspended in buffer containing SYTOX blue for dead cell exclusion and analyzed using a FACS Aria III (BD Biosciences). Cell debris were excluded by forward and side scatter gating. FlowJo was used for data analysis.

For intracellular flow cytometry mESCs were dissociated by Accutase (A6964, Sigma-Aldrich), centrifuged and resuspended in 2% of methanol-free formaldehyde (28906, Thermo Fisher Scientific) for 10 min in RT. Inside Stain kit (130-090-477, Miltenyi Biotec) was used according to manufacturer's protocol. Antibodies used are listed in the STAR Methods.

Subcellular fractionation of hESCs

5-10^6 cells were harvested, washed with ice-cold PBS and centrifuged at 500*g* 4°C. Cell pellets were gently resuspended in 380 μL cold cytoplasmic lysis buffer (50 mM Tris-pH 6.5, 100 mM NaCl, 300 mM Sucrose, 3 mM $MgCl_2$, 0.15% NP40) supplemented with 100 U RNasin Plus RNase inhibitor (PRN2615, Promega). After incubation on ice for 10 min, cells were briefly vortexed and centrifuged at 1000*g* 4°C for 3 min. The supernatant containing the cytoplasmic fraction was transferred, and centrifuged again at 4°C 5000*g* for 2 min to remove cell debris. Immediately after centrifugation 1 mL of RNA precipitation buffer (RPS; 9.5 mL 100% EtOH with 0.5 mL 3 M Sodiumacetate) was added and the supernatant was incubated at −20°C for 3 to 5 hours until further RNA purification.

The remaining pellet was washed three times with 400 μL cytoplasmic lysis buffer supplemented with an increasing concentrations 50 mM, 200 mM and 500 mM of Ammonium sulfate (for disrupting the endoplasmic reticulum attached to the nucleus but without breaking the nuclear envelope). For each washing step, the cell suspension was centrifuged at 4°C and 5000 *g* for 2 min and the supernatant was processed for RNA extraction.

380 μL of cold Modified Wuarin-Schibler (MWS) buffer (10 mM Tris-HCl pH 7.0, 4 mM EDTA, 0.3 M NaCl, 1 M Urea, 1% NP-40) supplemented with 100 U RNasin Plus RNase inhibitor was added to the remaining pellet. Samples were vortexed for 30 s, incubated on ice for 5 min, then vortexed again and kept on ice for 10 min. The suspension was centrifuged at 1000*g* 4°C for 3 min and the resulting supernatant representing the nucleoplasmic fraction was processed for RNA extraction.

The pellet was washed three times by adding 800 μL of MWS buffer, vortexing for 30 s and centrifuging at 500*g* 4°C for 2 min. 1 mL QIAzol (79306, QIAGEN) was added to the remaining chromatin pellet and after short vortexing, the suspension was stored at −20°C until further usage.

The RNA fraction in RPS buffer was vortexed for 30 s and after adding 1 μL Glycoblue coprecipitant (Life Technologies, AM9516) centrifuged at 18000 *g* 4°C for 15 min. 1 mL QIAzol was added to the partially air-dried pellet. 10 μL of 0.5 M EDTA was added to all samples and heated up to 65°C and incubated for 10 min to resuspend the pellet. After cooling down, 200 μL of chloroform / isoamyl alcohol (24:1) was added, the solution was vortexed for 30 s and then centrifuged at 18000 *g* RT for 10 min. The upper aqueous phase was transferred into a new tube and the same volume of isopropanol together with 1 μL of Glycoblue was added. After o/n incubation at −20°C, the samples were centrifuged at 18000 *g* RT. The pellets were washed once by adding 1 mL 70% EtOH and centrifuging at 18000 *g* RT for 5 min. Pellets were air-dried for 10 min and resuspended in RNase-free water. Cytoplasmic, nucleoplasmic and chromatin fractions were analyzed by RNA-sequencing as outlined above. Random primed, strand specific cDNA libraries were prepared following Illumina TruSeq total RNA protocol (above). 81 – 92% of obtained reads aligned to the human genome allowing a single mismatch.

QUANTIFICATION AND STATISTICAL ANALYSIS

Single molecule (sm)FISH and paraspeckle quantification

Based on Raj et al. (2008), h/mESCs that were grown on Matrigel coated sterile 2-well μ-Slides (80286, Ibidi) were washed twice for 5 min with 1x PBS, and fixed using 4% methanol-free formaldehyde (10321714, Thermo Fisher Scientific) for 10 min at RT. Following additional two wash steps, cells were permeabilized using 70% ethanol for 12 h at 4°C, and were washed twice again. Then preparations were incubated for 15 min with hybridization buffer prepared using 2x saline-sodium citrate (SSC) solution / 10% deionized formamide (4610-OP, Calbiochem). Hybridization with Stellaris FISH probes was done in a total volume of 50 μl hybridization buffer containing 50 μg competitor tRNA from *E.coli* (10109541001, Roche Diagnostics), 10% Dextran Sulfate (9011-18-1, VWR), 2 mg/ml

UltraPure BSA (AM2616, Thermo Fisher Scientific), and 10 mM vanadyl-ribonucleoside complex (S1402S, New England BioLabs) with probes at final concentration of 1 ng/μl. Preparations were covered with parafilm and incubated at 37°C for 5 h, and afterward washed twice with pre-warmed 2xSCC/10% formamide for 30 min at 37°C. Finally the preparations were washed twice with 1x PBS at RT, and then mounted using 10 μl ProLong Gold Antifade Reagent containing DAPI (9071S, New England Biolabs). The slides were imaged when the mounting medium was fully cured > 12 h.

Probes were designed using the Probe Designer software from Biosearch Technologies and were provided by same vendor. Probes included were hNEAT1 middle segment conjugated to Quasar570 (SMF-2037-1), human NEAT1 5' segment conjugated to Quasar670 or Quasar570 (SMF-2036-1), mouse Neat1 middle segment conjugated to Quasar670 and mNeat1 5' segment conjugated to Quasar570 (sequences of probes available upon request). Quantification of hybridization signal was performed using spot detection algorithm Airlocalize (Trcek et al., 2017).

RNA-FISH and immunofluorescence

RNA-FISH - immunofluorescence was performed as previously described (Kawaguchi et al., 2015; West et al., 2016). The RNA probes were synthesized using T7 or SP6 RNA polymerase and a digoxigenin (DIG) RNA labeling kit (11175025910, Roche). Linearized plasmids (1 μg) containing a NEAT1 fragment (NEAT1 1-1000 nt) were used as templates. Cells were grown on coverslips (Matsunami; micro cover glass; 18 mm round; thickness, 0.16–0.19 mm) and treated with 5 uM proteasome inhibitor (MG132, Sigma-Aldrich) for 6 h to enhance NEAT1 expression (Hirose et al., 2014). Then cells were fixed with 4% paraformaldehyde/PBS at room temperature for 10 min, washed using 1 × PBS, permeabilized with 0.5% Triton X-100 (9002-93-1, Sigma-Aldrich)/PBS for 5 min, and washed three times with 1 × PBS. Subsequently, the cells were dipped in 100% ethanol for 5 min and then dried. Dehydrated coverslips were incubated with pre-hybridization solution (50% formamide, 1 × Denhardt's salt, 2 × SSC, 100 mM EDTA, 100 ug/ml yeast tRNA, and 0.01% Tween 20) at 55°C for 1 h and then incubated with hybridization solution (as above with 5% Dextran sulfate) containing the DIG-labeled RNA probes (final concentration: 100 ng/coverslip) at 55°C o/n. After hybridization, the coverslips were washed twice with pre-warmed wash buffer (50% formamide, 2 × SSC, and 0.1% Tween 20) at 55°C for 15 min. Then, excess RNA probes were digested with 10 ug/ml RNase A (9001-99-4, Nacalai Tesque) in NTET buffer (10 mM Tris-HCl [pH 8.0], 1 mM EDTA, 500 mM NaCl, and 0.1% Tween 20) at 37°C for 30 min. The coverslips were washed with buffer (2 × SSC and 0.01% Tween 20) at 55°C for 15 min and washed twice with a second buffer (0.1 × SSC and 0.01% Tween 20) at 55°C for 15 min. The coverslips were subsequently washed with TBST (1 × TBS containing 0.1% Tween 20) and incubated with 1 × blocking solution (Blocking reagent [Roche] diluted with TBST) for blocking at RT for 1 h. Then, the coverslips were incubated with primary antibodies, Anti-Digoxigenin mouse monoclonal antibody (clone 21H8, Abcam), Anti-TDP-43 rabbit polyclonal antibody (Proteintech, 1:100), anti-PSPC1 rabbit polyclonal antibody (1:1000; Naganuma et al., 2012) in 1 × blocking solution at room temperature for 1 h, washed three times with TBST for 5 min, and incubated with secondary antibodies, anti-mouse IgG Alexa 488, and anti-rabbit IgG, Alexa-568 (both Thermo Fisher Scientific]) in 1 × blocking solution at RT for 30 min, and washed three times with TBST for 5 min. The coverslips were mounted with VECTASHIELD Hard Set Mounting Medium with DAPI (Vector). Confocal images were acquired using a confocal laser scanning microscope FV1000D (Olympus). Cells were automatically counted using Fiji software. First, nuclei or paraspeckles were segmented using either DAPI or FISH staining to identify areas of interest. Then gausian blur (1.2) was applied and threshold for each object was calculated using Otsu's method. Mean intensity values or correlation coefficients were measured for the respective areas.

iCLIP protocol and its analysis

The iCLIP protocol was performed as described previously (Huppertz et al., 2014) with several modifications. Cells were irradiated by UV once with 160 mJ/cm^2 using Stratalinker 1800 at 254 nm. TDP-43 was immunoprecipitated with protein A Dynabeads (10002D, Invitrogen) conjugated to rabbit-anti TDP-43 (Sigma-Aldrich, SAB4200006) or GFP (Life, Technologies, A6455). The region corresponding to 55–100kDa complexes was excised from the membrane to isolate the RNA, and sequenced using Illumina HiSeq, generating 50-nt single-end reads, sequencing depth was 15- 20 Mio reads per library. Analysis of reproducibility of cross-linked sites, identification of the significant iCLIP crosslinked clusters and z-score analysis of enriched pentamers was performed as described (Tollervey et al., 2011) and data was processed by the iCount software (https://github.com/tomazc/iCount).

RNA-Seq differential expression

To identify differentially expressed genes from RNA-Seq data, sequencing reads were mapped using TopHat2 (Trapnell et al., 2009), and gene count tables were produced using HTSeq and Ensembl genome version 74. Finally, edgeR (Robinson et al., 2010) was applied to analyze P value and fold-expression changes.

Identification of polyA sites

QuantSeq read data were aligned to hg19 reference genome with STAR (Dobin et al., 2013). Reads that did not align uniquely were filtered out. Identification of polyA-sites with QuantSeq relies on annealing of poly(T) primers to the polyA tails of mRNAs. To exclude cases of internal priming, where primer anneal to genomic polyA sequences, A-rich regions in vicinity of putative polyA sites were removed ([-10..10]). Additionally, only polyA-sites that were more than 125 nt apart from each other were treated separately, because

cleavage is not a nucleotide exact process, and therefore closely spaced polyA-site were pooled. PolyA site classification was done by including those sites that were adjacent to polyA-site signals [-100, 25] nt.

polyA sites were categorized based on presence of a preceding polyA signal using polyAR (Akhtar et al., 2010). Four classes were annotated, strong, weak, lacking polyA signal and non-categorized sites. The nucleotide composition, overlap with a published dataset of polyA-sites (Derti et al., 2012) and efficiency of cleavage (cDNA counts) for each class of sites was analyzed, and confirmed that strong and weak sites were the most reliable sites in terms of known nucleotide composition around polyA-sites.

Strong and weak polyA-sites were used to define position-dependent polyA-site regulation by TDP-43. Of a total 28,930 polyA sites (strong + weak), 23,309 sites were annotated to genes (Ensembl version 74). 17,286 polyA-site exhibited strong signals across experiments (a minimum of 10 reads needed to be detected in either test or control sample). Summing the counts across all experiments was used as an additional filtering step to avoid sites that resulted from inefficient cleavage. Only polyA sites that exhibited > 5% the level of another major site in the same gene were included. Since alternative long 3′ UTRs are not yet fully annotated, 5k of the intergenic region downstream of each gene were included in this analysis (however only to the middle of the downstream gene if distance < 5kb). This led to the identification of 16,065 sites in 10,661 genes presented in (Table S5).

Analysis of alternative polyadenylation (APA)

Genes included were those exhibiting two major pA-sites (highly expressed in both test and control). Next, pA-site pairs were classified as same-exon, composite-exon or skipped-exon. For same-exon sites, the major site was compared to the sum of all other sites within the same exon (exon level). For composite-exon and skipped-exon pairs, the major site was compared to the expression of the other sites in the gene.

To estimate the level of change in expression between control and test groups, we calculated the "percent change" (pc) score, as follows:

$$pc = control_{PROXIMAL}/control_{PROXIMAL+DISTAL} - test_{PROXIMAL}/test_{PROXIMAL+DISTAL}[-1, 1]$$

Positive values determine a higher ratio of control versus test in proximal versus distal sites, and the negative values represent the opposite trend. Fisher's exact test was then used to determine the significance of the change. Genes were regarded as displaying significant changes in polyA site usage between test and control is Fisher's p value was < 0.1. Lastly genes were classified as repressed (pc < −0.1), enhanced (pc > 0.1) and controls (abs(pc) < 0.1 and p value > 0.1). GO-term analysis of TDP-43 regulated alternatively polyadenylated transcripts was performed based on Blake et al. (2015).

Visualizing position-dependent polyA site regulation using RNA-maps

After identifying genes exhibiting APA, summed crosslinked sites derived from iCLIP were plotted around the pA sites of repressed, enhanced and control genes (Figures S5E–S5G). This RNA-map approach is similar to plotting RNA-maps around splice sites in alternative-splicing context (Ule et al., 2006; Witten and Ule, 2011).

mRNA/RBP occupancy (mRNA interactome capture)

Protocol was based on Castello et al. (2013). ~50X10^6 undifferentiated cells in 3 replicates of WT hESC and *NEAT1ΔpA* hESC were irradiated as described for iCLIP.

FASP digest

Each 10μg of RBPome were digested with a modified FASP procedure (Wiśniewski et al., 2009). Briefly, the proteins were reduced and alkylated using dithiothreitol and iodoacetamide, diluted with one volume of UA buffer (8 M urea in 0.1M Tris/HCl pH 8.5) and then centrifuged through a 30 kDa cut-off filter device (PALL, Port Washington). Samples were washed twice with UA buffer and twice with 50 mM ammonium bicarbonate prior to digest of the immobilized proteins on the filter for 2 h at RT using 1 μg Lys-C (Wako Chemicals) and for 16 h at 37°C using 2 μg trypsin (Promega). Tryptic peptides were collected by centrifugation (10 min at 14,000 g), and the samples were acidified with 0.5% TFA and stored at −20°C.

Mass spectrometry

Before loading, the samples were centrifuged for 5 min at 4°C. LC-MS/MS analysis was performed on a QExactive HF mass spectrometer (Thermo Scientific) online coupled to an Ultimate 3000 nano-RSLC (Thermo Scientific). Approximately 0.5 μg of every digested sample was automatically injected and loaded onto the trap column at a flow rate of 30 μl/min in 3% ACN/ 0.1% FA. After 5 min, the peptides were eluted from the trap column and separated on the C18 analytical column (75 μm i.d. x 25 cm, Acclaim PepMap100 C18.2 μm, 100Å, Dionex) by a 90 min gradient from 5 to 25% ACN in 0.1% FA at 300 μl/min flow rate followed by a 5 min gradient from 25% to 40% ACN in 0.1% FA. Between each sample, the column was washed with 85% ACN for 5 min followed by equilibration at 3% ACN in 0.1% FA for 18 min. MS spectra were recorded at a resolution of 60000 with an AGC target of 3e6 and a maximum injection time of 50 ms from 300 to 1500 m/z. From the MS scan, the 10 most abundant peptide ions were selected for fragmentation via HCD with a normalized collision energy of 27, an isolation window of 1.6 m/z and a dynamic exclusion of 30 s. MS/MS spectra were recorded at a resolution of 15000 with a AGC target of 1e5 and a maximum injection time of 50 ms. Intensity threshold was set to 1e4and unassigned charges and charges of +1 and > 8 were excluded.

Analysis of mRNA-interactome

Progenesis QI software (version 2.0, Nonlinear Dynamics) was used for label free quantification as described previously (Merl et al., 2012). Briefly, profile data of the MS and MS/MS scans were transformed to peak lists with respective peak m/z values, intensities, abundances (areas under the peaks) and m/z width. After reference selection, the retention times of the other samples were aligned by automatic alignment to a maximal overlay of all features. After exclusion of all features with only one charge or more than seven charges, all remaining MS/MS spectra were exported as Mascot generic file and used for peptide identification with Mascot (version 2.5.1) in the Ensembl Human protein database. Search parameters used were: 10 ppm peptide mass tolerance and 20 mmu fragment mass tolerance, one missed cleavage allowed, carbamidomethylation was set as fixed modification, methionine oxidation and asparagine or glutamine deamidation were allowed as variable modifications. A Mascot-integrated decoy database search calculated an average false discovery of 1% when searches were performed with a mascot percolator score cut-off of 13 and an appropriate significance threshold p. Peptide assignments were re-imported into the Progenesis QI software and the abundances of all peptides allocated to each protein were summed up. Resulting normalized protein abundances were used further and compared to existing mRNA-interactome datasets obtained from HeLa (Castello et al., 2012) and HEK293 cells (Baltz et al., 2012). As the aim of this study was not to expand the repertoire of RBPs, but rather to determine the dynamics of high confidence RBPs bound to mRNAs, we used only the overlap between published and our datasets (388 high confidence RBPs) for analysis of mRNA interactome changes upon gain of paraspeckles in *NEAT1ΔpA* cells compared to the parental line.

DATA AND SOFTWARE AVAILABILITY

Raw sequencing files (50 nt, single-end) have been deposited in the ArrayExpress archive (accessible at E-MTAB-5090; E-MTAB-5091; E-MTAB-5097; E-MTAB-5099; E-MTAB-5100; E-MTAB-5114, E-MTAB-5115, E-MTAB-5116) and https://expressrna.org/ platform that enables visualization and accession of the sequencing data. Similarly, iCLIP data are deposited and available also in https://imaps.genialis.com/ and validation of CRISPR-Cas9 modified cell lines are deposited to Mendeley data (https://data.mendeley.com/datasets/hbr8p7n526/2).